

Coordinated Multi-Robot Trajectory Tracking over Sampled Communication [★]

Enrica Rossi ^a, Marco Tognon ^b, Luca Ballotta ^a, Ruggero Carli ^a, Juan Cortés ^c,
Antonio Franchi ^{c,d}, Luca Schenato ^a

^a*Department of Information Engineering, University of Padova, Italy*

^b*Autonomous Systems Lab, Department of Mechanical and Process Engineering, ETH Zurich, 8092 Zürich, Switzerland*

^c*LAAS-CNRS, Université de Toulouse, CNRS, Toulouse, France*

^d*Robotics and Mechatronics lab, University of Twente, Enschede, The Netherlands*

Abstract

In this paper, we propose an inverse-kinematics controller for a class of multi-robot systems in the scenario of sampled communication. The goal is to make a group of robots perform trajectory tracking in a coordinated way when the sampling time of communications is non-negligible, disrupting the theoretical convergence guarantees of standard control designs. Given a feasible desired trajectory in the configuration space, the proposed controller receives measurements from the system at sampled time instants and computes velocity references for the robots, which are tracked by a low-level controller. We propose a jointly designed feedback plus feedforward controller with provable stability and error convergence guarantees, and further show that the obtained controller is amenable of decentralized implementation. We test the proposed control strategy via numerical simulations in the scenario of cooperative aerial manipulation of a cable-suspended load using a realistic simulator (*Fly-Crane*). Finally, we compare our proposed decentralized controller with centralized approaches that adapt the feedback gain online through smart heuristics, and show that it achieves comparable performance.

Key words: Autonomous systems; control over sampled communications; cooperative control; trajectory tracking.

1 Introduction

Unmanned Aerial Vehicles (UAVs) are used in the context of mobile robotics to perform surveillance, coverage, exploration, and transportation [17]. Generally speaking, a group of robots allows to improve task performance with respect to (w.r.t.) the single-robot solution. The use of multiple robots can mitigate problems as the

limited payload and time of flight [2]. However, they require careful consideration of cooperation or coordination strategies to achieve common goals [6]. Consider a group of UAVs that transports a load while avoiding obstacles or passing through narrow apertures. In this case, not only each UAV has to avoid obstacles, but also the overall multi-robot system should move in a coordinated way such that the load avoids obstacles, as well [4].

One of the most direct approaches to control multi-robot systems is the centralized kinematic/dynamic inversion [1, 15, 16, 23, 28]. Because of its nature, failure of the central unit may cause the whole task to fail. Distributed and decentralized approaches spread computations across the robots, guaranteeing greater robustness and flexibility w.r.t. a centralized one [22]. Although such approaches are preferable for multi-robot systems, they often lack global information as the load state and parameters, or the total number of robots. This aspect increases the difficulty of the controller design and might even degrade performance. Examples of

[★] This work Partially funded by: the European Commission project H2020 AERIAL-CORE (EC 871479), the ANR, Project ANR-17-CE33-0007 MuRoPhen and by University of Padova grant “Magic” SCHE.SID17_01.

Email addresses: enrica.rossi.1@studenti.unipd.it (Enrica Rossi), mtognon@ethz.ch (Marco Tognon), ballotta@dei.unipd.it (Luca Ballotta), carlirug@dei.unipd.it (Ruggero Carli), juan.cortes@laas.fr (Juan Cortés), antonio.franchi@laas.fr, a.franchi@utwente.nl (Antonio Franchi), schenato@dei.unipd.it (Luca Schenato).

distributed control methods can be found for groups of ground [5, 10, 19, 20], underwater [3, 27], and aerial robots [18]. The mentioned approaches are based on the explicit exchange of data among the robots. Examples of decentralized approaches involving ground or aerial manipulators can be found in [26] and [33]. To reduce communication issues, communication-less approaches relying on a leader-follower paradigm were presented for the problem of cooperative transportation and manipulation [7, 11, 30, 32, 34]. In these cases, communication is implicit and exploits the forces exerted on the load [31]. However, force feedback may be insufficient for precise tracking, because it lacks pose information. This can be retrieved by implementing communication among the robots, e.g., exchanging their pose, or installing a sensor on the load broadcasting its pose. This setup can also be extended to formation control problems where a group of robots must complete a task [8, 9]. For example, a common goal may be mapping or surveillance of an area while the robots must keep a certain 3D formation in order to, e.g., minimizing the overlap of the robots' fields of view [24]. In this case, a communication-based approach allows the robots to exchange measurements about the formation of the group, as relative distances.

In real applications, the limited bandwidth of wireless communication channels disrupts the common assumption of continuous-measurement feedback. As so, specific strategies are needed to deal with sampled communication [12, 14, 29]. However, little work is currently available in the context of multi-robot manipulation. In [21], the authors investigated the problem of coordinated aerial load transportation with sampled communication. Considering the problem of rest-to-rest motions, they designed an online inverse-kinematic controller that moves the system from an initial to a final configuration with zero velocity. During the motion, the method proposed in [21] updates the reference velocities for the robots every time a new state measurement arrives. The behavior of the system under sampled communication (e.g., when the desired robots velocities are transmitted via Wi-Fi) was analyzed. An offline strategy and an online one were proposed to design the controller gain, with different implementations and convergence guarantees. For both cases, stability and at least exponential convergence were proved, regardless of the sampling period.

1.1 Preview of Key Results

In this paper, we aim to design a multi-robot decentralized controller when wireless communication induces non-negligible sampling of feedback measurements. In this context, a decentralized implementation is preferred because it i) reduces the overall communication burden, and thus related issues as packet loss or latency, and ii) enhances system robustness and scalability. Previous work [21] is limited to point-stabilization, which strongly restricts its applicability. As a prelimi-

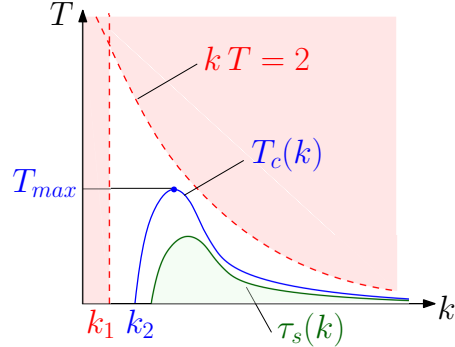


Fig. 1. We propose a controller for trajectory tracking when measurements are transmitted with sampling time T . We show that, if (k, T) belongs to the red area, with k the feedback gain, the tracking error may not converge, while zero tracking error is guaranteed if (k, T) is below the blue curve.

nary step, we show that the controller developed in [21] cannot guarantee zero tracking error for arbitrary reference trajectories. Thus, we propose a novel *Sampled communication-aware Inverse-Kinematic controller for Multi-robot systems* (SIKM) to address the challenging problem of trajectory tracking under sampled communication. Our contributions are summarized as follows.

- We propose a general model that includes different multi-robot systems, ranging from teams of UAVs for cooperative manipulation of cable-suspended loads, to teams of generic robots for formation control.
- We develop a decentralized SIKM controller for trajectory tracking that receives sampled measurements and generates the desired robot velocities along the whole trajectory, exploiting a novel formulation of the feedforward term that tames sampled communication.
- We show that, for any feasible sampling time, the feedback gain must belong to a bounded interval in order to stabilize the system, and provide a numerical procedure to estimate the set of stabilizing gains (Fig. 1).
- We formally prove that the proposed SIKM controller guarantees asymptotic stability and zero tracking error in the absence of external disturbances.

To validate our strategy, we test the controller on a dynamic simulator which replicates with high accuracy the experimental setup available at the LAAS-CNRS Lab, named *Fly-Crane* [23], including sensor noise and real-time embedded software implementation. Further, we compare our approach to centralized controllers that compute the feedback gain online by exploiting smart heuristics based on the method in [21], and show that our decentralized strategy provides superior or comparable performance to such centralized approaches.

1.2 Paper Outline

In Sec. 2, we introduce the class of multi-robot systems considered in this work, defining the kinematic model

(Sec. 2.1) and providing examples of real systems that are represented by such a model (Sec. 2.2). In Sec. 2.3, we formalize the trajectory tracking problem, showing that, when measurements are continuously available, perfect tracking can be achieved easily. In Sec. 3, we introduce the SIKM controller to perform trajectory tracking with sampled communication. In Sec. 4, we explicitly find the set of controller parameters that guarantee system stability and the fastest convergence rate of the error. In Sec. 5, we test our control strategy on the realistic *Fly-Crane* dynamic simulator, and show that it outperforms both the technique presented in [21] and the naive feed-forward design. Concluding remarks are drawn in Sec. 6.

2 System Model and Problem Formulation

2.1 Kinematics of Multi-Robot Systems

In this section, we describe the kinematic model of a multi-robot system composed of N robots that coordinated their motions via state information exchanged with a common *pivot*, labeled as V , to fulfill a task. As so, the robots do not communicate among themselves, thus reducing communication burden. This can be an object to be manipulated, a robot to be escorted, or a vehicle in the space. The kinematic model is given by

$$[\mathbf{p}_1 \ \dots \ \mathbf{p}_N]^\top = \mathbf{h}(\mathbf{q}) = [\mathbf{h}^{(1)}(\mathbf{q}_1, \mathbf{q}_V) \ \dots \ \mathbf{h}^{(N)}(\mathbf{q}_N, \mathbf{q}_V)]^\top. \quad (1)$$

This function maps the Lagrangian coordinates of the system $\mathbf{q} = [\mathbf{q}_1^\top \ \dots \ \mathbf{q}_N^\top \ \mathbf{q}_V^\top]^\top \in \mathbb{R}^m$ to the vector collecting the robots configurations $\mathbf{p} = [\mathbf{p}_1^\top \ \dots \ \mathbf{p}_N^\top]^\top \in \mathbb{R}^n$. In particular, $\mathbf{p}_i \in \mathbb{R}^{n_i}$ is the position of the i -th robot in space, $\mathbf{q}_i \in \mathbb{R}^{m_i}$ gathers the angles and/or distances between the pivot V and the i -th robot, and $\mathbf{q}_V \in \mathbb{R}^{m_V}$ represents the pose (position and orientation) of the pivot itself. Notice that $m = \sum_{i=1}^N m_i + m_V$ and $n = \sum_{i=1}^N n_i$. The differential kinematics of the system is:

$$\dot{\mathbf{p}} = \mathbf{A}_{\mathbf{q}} \dot{\mathbf{q}}, \quad (2)$$

where the Jacobian $\mathbf{A}_{\mathbf{q}} = \frac{\partial \mathbf{h}(\mathbf{q})}{\partial \mathbf{q}} \in \mathbb{R}^{n \times m}$ has structure

$$\mathbf{A}_{\mathbf{q}} = \begin{bmatrix} \mathbf{A}_{\mathbf{q}_1}^{(1)} & \mathbf{0} & \mathbf{A}_{\mathbf{q}_V}^{(1)} \\ & \ddots & \vdots \\ \mathbf{0} & \mathbf{A}_{\mathbf{q}_N}^{(N)} & \mathbf{A}_{\mathbf{q}_V}^{(N)} \end{bmatrix}, \quad (3)$$

$\mathbf{A}_{\mathbf{q}_i}^{(i)} = \frac{\partial \mathbf{h}^{(i)}(\mathbf{q}_i, \mathbf{q}_V)}{\partial \mathbf{q}_i} \in \mathbb{R}^{n_i \times m_i}$ and $\mathbf{A}_{\mathbf{q}_V}^{(i)} = \frac{\partial \mathbf{h}^{(i)}(\mathbf{q}_i, \mathbf{q}_V)}{\partial \mathbf{q}_V} \in \mathbb{R}^{n_i \times m_V}$. We will focus on the case $n = m$, corresponding to *square systems*. Let us make an example to justify this choice. Consider a multi-robot system as the one in Fig. 2a where the robots are linked to a platform through rigid cables; assume that $\mathbf{A}_{\mathbf{q}}$ is invertible and that the input to the system is the vector of desired robots velocities

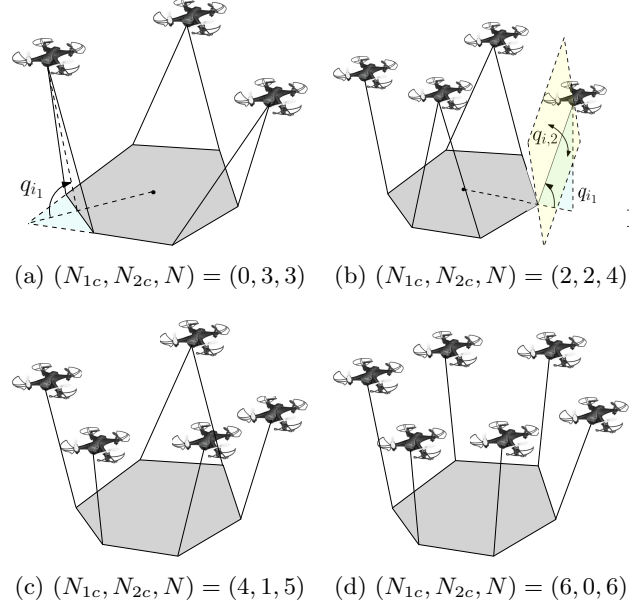


Fig. 2. Square systems where a common object is manipulated by a group of UAVs. All the possible combinations of (N_{1c}, N_{2c}, N) introduced in Sec. 2.2 are represented.

$\dot{\mathbf{p}}^d$. If $n = m$, there always exists a vector $\dot{\mathbf{q}} = \mathbf{A}_{\mathbf{q}}^{-1} \dot{\mathbf{p}}^d$ in the configuration space that allows the robots to achieve the desired velocity. Conversely, if $n \neq m$, the Jacobian is not square. In particular, the system is redundant if $n > m$. If $n < m$, there exist trajectories in the configuration space $\dot{\mathbf{q}}$ which are infeasible for any input $\dot{\mathbf{p}}^d$. Such cases require a dedicated analysis which goes beyond the scope of this paper. [We refer to \[?\] for such an analysis, that, with some attention, allows to integrate the control strategy proposed here into more general systems.](#)

Furthermore, we do not consider the system dynamics because its effects can be neglected for quasi-static motions which are the most common in practical scenarios. This translates into a simpler design of the controller at the kinematic level. Nevertheless, we tested the proposed controller on a full dynamical model of the system.

2.2 Examples of Square Systems

In the literature, we can find several examples of square systems. One is the multi-robot system depicted in Fig. 2a (called *Fly-Crane* [15]), where three UAVs transport a common platform. Each robot is linked to the load through two rigid cables. The generalized coordinates are chosen as $\mathbf{q} = [q_1 \ q_2 \ q_3 \ \mathbf{q}_V^\top]^\top$. The robot positions $\mathbf{p}_i \in \mathbb{R}^3$ are collected in the vector $\mathbf{p} = [\mathbf{p}_1^\top \ \mathbf{p}_2^\top \ \mathbf{p}_3^\top]^\top$. Thus, the velocity vectors $\dot{\mathbf{q}}, \dot{\mathbf{p}} \in \mathbb{R}^9$ have the same dimension and $\mathbf{A}_{\mathbf{q}} \in \mathbb{R}^{9 \times 9}$ is a square matrix. However, this is a particular case of a larger class: different square systems can be obtained by simply changing the number of robots transporting the platform or the number of cables linking each robot to it. Notice that if one ca-

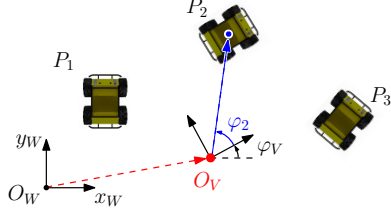


Fig. 3. Representation of a multi-robot system where three robots must keep the same orientation φ_i w.r.t. the reference frame centered in the point O_c during the assigned task.

ble was used instead of two, as shown in Fig. 2b, then $\mathbf{q}_i = [q_{i1} \ q_{i2}]^\top \in \mathbb{R}^2$ because each cable can move in two directions (assuming that movements about the cable axis are not allowed). In this case, the system is no more guaranteed to be square. In particular, it holds $n = 3N$ and $m = 6 + 2N_{1c} + N_{2c}$ where $N_{1c} \geq 0$ is the number of robots linked to the load through one cable and $N_{2c} \geq 0$ indicates the number of robots linked through two cables. We have that $N = N_{1c} + N_{2c}$ and, for a square system $n = m$, it must be $3N = 6 + 2N_{1c} + N_{2c}$. From these relations it turns out that $N_{2c} \leq 3$, $N_{1c} \leq 6$ and $N \leq 6$; in particular, the possible configurations (N_{1c}, N_{2c}, N) are: (0,3,3) in Fig. 2a, (2,2,4) in Fig. 2b, (4,1,5) in Fig. 2c, (6,0,6) in Fig. 2d.

Other examples of square systems are found in the context of formation control problems [9], as the one represented in Fig. 3. Three ground robots move in a 2-dimensional space while respecting some constraints w.r.t. the frame $\mathcal{F}_V = \{O_V, \mathbf{x}_V, \mathbf{y}_V\}$ representing the pivot (e.g., the barycenter of the system). The position P_i of each robot, defined by the vector $\mathbf{p}_i = [x_i \ y_i]^\top$, is described as a function of: the pivot position $\mathbf{p}_V = [x_V \ y_V]^\top$, the distance d_i from P_i to O_V , the angle φ_i between the line $O_V - P_i$ and the axis \mathbf{x}_V , and the angle φ_V between \mathbf{x}_V and \mathbf{x}_W of the world reference frame $\mathcal{F}_W = \{O_W, \mathbf{x}_W, \mathbf{y}_W\}$. It is trivial to express the position P_i w.r.t. \mathcal{F}_W :

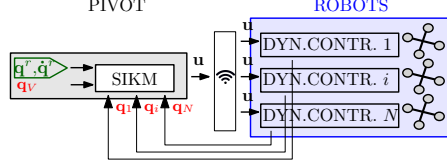
$$\mathbf{p}_i = \mathbf{h}(\mathbf{q}_i, \mathbf{q}_V),$$

where $\mathbf{q}_i = [d_i \ \varphi_i]^\top \in \mathbb{R}^2$, $\mathbf{q}_V = [x_V \ y_V \ \varphi_V]^\top \in \mathbb{R}^3$ and

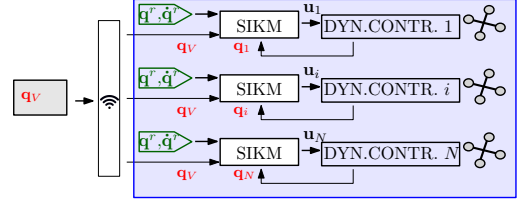
$$\mathbf{h}(\mathbf{q}_i, \mathbf{q}_V) = \begin{bmatrix} x_V \\ y_V \end{bmatrix} + \begin{bmatrix} \cos(\varphi_V) & -\sin(\varphi_V) \\ \sin(\varphi_V) & \cos(\varphi_V) \end{bmatrix} \begin{bmatrix} d_i \cos(\varphi_i) \\ d_i \sin(\varphi_i) \end{bmatrix}.$$

Let us define the vector of robot positions as $\mathbf{p} = [\mathbf{p}_1^\top \ \mathbf{p}_2^\top \ \mathbf{p}_3^\top]^\top \in \mathbb{R}^6$ and the vector of generalized coordinates as $\mathbf{q} = [\mathbf{q}_1^\top \ \mathbf{q}_2^\top \ \mathbf{q}_3^\top \ \mathbf{q}_V^\top]^\top \in \mathbb{R}^9$. Hence, we can write $\mathbf{h}(\mathbf{q}) \stackrel{\text{def}}{=} [\mathbf{h}(\mathbf{q}_1, \mathbf{q}_V)^\top \ \mathbf{h}(\mathbf{q}_2, \mathbf{q}_V)^\top \ \mathbf{h}(\mathbf{q}_3, \mathbf{q}_V)^\top]^\top$. We assume that the robots must perform a task while keeping the angles φ_i constant w.r.t. \mathcal{F}_V , hence the differential kinematic model is:

$$\dot{\mathbf{p}} = \mathbf{A}_q \dot{\mathbf{q}}',$$



(a) Centralized feedback, equation (5).



(b) Sparse feedback, equation (6).

Fig. 4. Possible implementations of the SIKM. The pivot is colored in gray, each robot (equipped with a dynamical controller which converts \mathbf{u} to forces) in blue, sensor measurements in red and the desired trajectory in green. The wireless symbol refers to sampled communication.

where $\dot{\mathbf{q}}' = [\dot{\mathbf{q}}_V^\top \ \dot{d}_1 \ \dot{d}_2 \ \dot{d}_3]^\top$ and

$$\mathbf{A}_q = \begin{bmatrix} \frac{\partial \mathbf{h}(\mathbf{q})}{\partial \mathbf{q}_V} & \frac{\partial \mathbf{h}(\mathbf{q})}{\partial d_1} & \frac{\partial \mathbf{h}(\mathbf{q})}{\partial d_2} & \frac{\partial \mathbf{h}(\mathbf{q})}{\partial d_3} \end{bmatrix} \in \mathbb{R}^{6 \times 6},$$

is a square matrix, hence this system is square, too.

The previous examples show that the considered class of square systems includes many relevant applications.

2.3 Problem Formulation

We consider a trajectory tracking problem where a multi-robot system is required to follow a sequence of desired configurations and velocities $(\mathbf{q}^r(t), \dot{\mathbf{q}}^r(t))$, $t \geq 0$, assigned *a priori*. We assume that the reference trajectory is generated by a planner that takes into account high-level goals such as obstacle and singularity avoidance, and energy minimization. Also, we assume that all robots are equipped with dynamical controllers sufficiently fast w.r.t. the dynamics of the system, such that (s.t.) their velocities are fully controllable,

$$\dot{\mathbf{p}}(t) = \mathbf{u}(t), \quad (4)$$

where $\mathbf{u} = [\mathbf{u}_1^\top \ \dots \ \mathbf{u}_N^\top]^\top \in \mathbb{R}^n$. We consider the following two architectures to implement the SIKM controller:

$$\mathbf{u}_i(t) = \kappa_i^c(\mathbf{q}(t); \mathbf{q}^r(t), \dot{\mathbf{q}}^r(t)), \quad (5)$$

$$\mathbf{u}_i(t) = \kappa_i^s(\mathbf{q}_i(t), \mathbf{q}_V(t); \mathbf{q}_i^r(t), \mathbf{q}_V^r(t), \dot{\mathbf{q}}_i^r(t), \dot{\mathbf{q}}_V^r(t)). \quad (6)$$

Specifically, $\mathbf{u}_i(t)$ depends on the full vector $\mathbf{q}(t)$ in (5), named *centralized feedback*, while it does not depend on $\mathbf{q}_j(t)$, $j \neq i$, in (6), named *sparse feedback*. Figure 4

shows two possible implementations. In Fig. 4a, the centralized SIKM controller is implemented on the pivot and receives all state measurements $\mathbf{q}(t)$. Then, the computed input $\mathbf{u}(t)$ is sent via wireless to the robots. By contrast, in the sparse implementation (Fig. 4b), the controllers are located on the robots and receive via wireless only the pivot pose. We will prove that, even in the realistic scenario where $\mathbf{q}(t)$ is sampled, it is still possible to design a sparse implementation (6) that guarantees stability and asymptotic zero tracking error by decoupling a centralized control law. This is attractive in making the system robust and scalable, and undertakes wireless communication issues, such as packet loss and latency, the centralized control is prone to.

In [21, Proposition 1], the authors showed that the controller

$$\mathbf{u}(t) = -k\mathbf{A}_{\mathbf{q}(t)}(\mathbf{q}(t) - \mathbf{q}^r) := \mathbf{u}_k(t), \quad k > 0, \quad (7)$$

drives the state $\mathbf{q}(t)$ to the desired constant configuration \mathbf{q}^r exponentially fast. In order to track a trajectory, the feedforward velocity term

$$\mathbf{u}_{\text{ff}}(t) = \mathbf{A}_{\mathbf{q}(t)}\dot{\mathbf{q}}^r(t),$$

is typically added to the feedback control input $\mathbf{u}_k(t)$ [25]. Indeed, by applying the control law

$$\mathbf{u}(t) = \mathbf{u}_k(t) + \mathbf{u}_{\text{ff}}(t), \quad (8)$$

the kinematics of system becomes

$$\dot{\mathbf{q}}(t) = -k(\mathbf{q}(t) - \mathbf{q}^r(t)) + \dot{\mathbf{q}}^r(t).$$

Defining $\mathbf{e}(t) \stackrel{\text{def}}{=} \mathbf{q}(t) - \mathbf{q}^r(t)$, we get

$$\dot{\mathbf{e}}(t) = \dot{\mathbf{q}}(t) - \dot{\mathbf{q}}^r(t) = -k(\mathbf{q}(t) - \mathbf{q}^r(t)) = -k\mathbf{e}(t),$$

which shows that the error goes exponentially fast to zero if $k > 0$. Moreover, notice that we can write (cf. (3))

$$\begin{aligned} \mathbf{u}_i(t) = & -k\mathbf{A}_{\mathbf{q}_i(t)}^{(i)}(\mathbf{q}_i(t) - \mathbf{q}_i^r(t)) - k\mathbf{A}_{\mathbf{q}_V(t)}^{(i)}(\mathbf{q}_V(t) - \mathbf{q}_V^r(t)) \\ & + \mathbf{A}_{\mathbf{q}_i(t)}^{(i)}\dot{\mathbf{q}}_i^r(t) + \mathbf{A}_{\mathbf{q}_V(t)}^{(i)}\dot{\mathbf{q}}_V^r(t). \end{aligned} \quad (9)$$

Since the controller (9) exhibits the decoupled structure (6), a sparse implementation is possible.

When measurements are sampled, modifying the feedback and feedforward terms in (8) such that the tracking error goes to zero is nontrivial. If \mathbf{q} is sampled and transmitted every T seconds, the authors in [21] proposed the following modification of (7) for point-stabilization:

$$\mathbf{u}(t) = \mathbf{u}_k(hT) = -k\mathbf{A}_{\mathbf{q}(hT)}(\mathbf{q}(hT) - \mathbf{q}^r), \quad (10)$$

for $t \in [hT, (h+1)T)$, $h \in \mathbb{N}$. Under mild assumptions, (10) drives \mathbf{q} to a constant reference \mathbf{q}^r exponentially fast. In this paper, we will show how to improve the controller (10) to track time-varying trajectories $\mathbf{q}^r(t)$. To this aim, we make the following assumptions.

Assumption 1 *The following relations hold.*

- i) *The reference trajectory $\mathbf{q}^r(t) \in \mathcal{Q}$ is twice continuously differentiable and \mathcal{Q} is a compact set. Moreover, velocities and accelerations are uniformly bounded, i.e., $\|\dot{\mathbf{q}}^r(t)\| \leq v_{\max}$ and $\|\ddot{\mathbf{q}}^r(t)\| \leq a_{\max}$.*
- ii) *There exists $d > 0$ such that, for any $\mathbf{q}^r(t)$ and \mathbf{q} being at distance smaller than d from the trajectory to be followed, i.e., $\|\mathbf{q} - \mathbf{q}^r(t)\| < d$, $\mathbf{A}_{\mathbf{q}}$ is twice continuously differentiable and invertible.*
- iii) *$\|\mathbf{q}(0) - \mathbf{q}^r(0)\| < d$.*

Assumption 1.i) are smoothness properties of the reference trajectory needed to derive error bounds. Assumption 1.ii) is necessary to guarantee that the reference trajectory is bounded away from singularities, thus ensuring robustness to, e.g., external disturbances, and can be accommodated through an offline high-level planner. Assumption 1.iii) is required to avoid that the initial condition is a singularity point. We will later show that our proposed control strategies, under such assumptions, also guarantees that the trajectory is always bounded away from singularities.

3 SIKM: Feedback-Feedforward Technique

In this section, we show how to improve the control law (10) in order to track time-varying trajectories $\mathbf{q}^r(t)$. In the first place, the feedback term is adjusted to embed trajectory samples $\mathbf{q}^r(hT)$, that are updated at each sampling instant, in place of the constant reference \mathbf{q}^r :

$$\mathbf{u}(t) = \mathbf{u}_k(hT) = -k\mathbf{A}_{\mathbf{q}(hT)}(\mathbf{q}(hT) - \mathbf{q}^r(hT)). \quad (11)$$

It can be shown that such a strategy yields bounded error, which however does not converge to zero.¹ This should not surprise: indeed, the feedback controller (11) tracks points which change at a fixed rate, preventing the error to go to zero when the trajectory gets close to the given reference. The proof is available in Appendix B. Thus, the addition of a feedforward term is needed to drive the error to zero. A first, naive attempt is to sample the control law (8):

$$\begin{aligned} \mathbf{u}(hT + \tau) = & -k\mathbf{A}_{\mathbf{q}(hT)}(\mathbf{q}(hT) - \mathbf{q}^r(hT)) + \\ & + \mathbf{A}_{\mathbf{q}(hT)}\dot{\mathbf{q}}^r(hT + \tau), \end{aligned} \quad (12)$$

¹ Indeed, it is commonly used in robotic applications.

where $\tau \in [0, T)$ and $\dot{\mathbf{q}}^r(hT + \tau)$ is assumed to be continuously available². Noting that $\mathbf{q} = \mathbf{e} + \mathbf{q}^r$, (12) becomes

$$\mathbf{u}(hT + \tau) = \mathbf{A}_{\mathbf{e}(hT) + \mathbf{q}^r(hT)}(-k\mathbf{e}(hT) + \dot{\mathbf{q}}^r(hT + \tau)),$$

and the evolution of $\mathbf{q}(\cdot)$ is

$$\dot{\mathbf{q}}(hT + \tau) = \mathbf{A}_{\mathbf{e}(hT + \tau) + \mathbf{q}^r(hT + \tau)}^{-1} \mathbf{u}(hT + \tau),$$

while the error dynamics $\dot{\mathbf{e}} = \dot{\mathbf{q}} - \dot{\mathbf{q}}^r$ becomes

$$\begin{aligned} \dot{\mathbf{e}}(hT + \tau) &= -k\mathbf{A}_{\mathbf{e}(hT + \tau) + \mathbf{q}^r(hT + \tau)}^{-1} \mathbf{A}_{\mathbf{e}(hT) + \mathbf{q}^r(hT)} \mathbf{e}(hT) + \\ &+ (\mathbf{A}_{\mathbf{e}(hT + \tau) + \mathbf{q}^r(hT + \tau)}^{-1} \mathbf{A}_{\mathbf{e}(hT) + \mathbf{q}^r(hT)} - \mathbf{I}) \dot{\mathbf{q}}^r(hT + \tau). \end{aligned}$$

Proposition 1 *Under control strategy (12), the reference trajectory is not an equilibrium trajectory, i.e.,*

$$\mathbf{q}(t) = \mathbf{q}^r(t) \not\Rightarrow \dot{\mathbf{e}}(t) = 0, \forall t \geq 0.$$

PROOF. If $\mathbf{q}(t) = \mathbf{q}^r(t)$, then $\mathbf{e}(t) = 0$ and

$$\dot{\mathbf{e}}(hT + \tau) = (\mathbf{A}_{\mathbf{q}^r(hT + \tau)}^{-1} \mathbf{A}_{\mathbf{q}^r(hT)} - \mathbf{I}) \dot{\mathbf{q}}^r(hT + \tau),$$

which is nonzero for all $h \in \mathbb{N}$ and $\tau \in (0, T)$ unless $\dot{\mathbf{q}}^r(t) \equiv \mathbf{0}$, i.e., the reference trajectory is constant. \square

The previous result shows that sampling the continuous-time law (8) does not guarantee perfect tracking. We propose to modify the feedforward term in order to guarantee perfect (asymptotic) tracking. Assuming that a desired trajectory $(\mathbf{q}^r(\cdot), \dot{\mathbf{q}}^r(\cdot))$ is given as reference, we choose a new control law for the SIKM controller:

$$\begin{aligned} \mathbf{u}(hT + \tau) &= -k\mathbf{A}_{\mathbf{q}(hT)}(\mathbf{q}(hT) - \mathbf{q}^r(hT)) + \\ &+ \mathbf{A}_{\mathbf{q}^r(hT + \tau)} \dot{\mathbf{q}}^r(hT + \tau). \end{aligned} \quad (13)$$

Differently from (12), the Jacobian of the feedforward term is computed at $\mathbf{q}^r(hT + \tau)$ instead of $\mathbf{q}(hT)$. Accordingly, the error dynamics becomes

$$\begin{aligned} \dot{\mathbf{e}}(hT + \tau) &= -k\mathbf{A}_{\mathbf{e}(hT + \tau) + \mathbf{q}^r(hT + \tau)}^{-1} \mathbf{A}_{\mathbf{e}(hT) + \mathbf{q}^r(hT)} \mathbf{e}(hT) + \\ &+ (\mathbf{A}_{\mathbf{e}(hT + \tau) + \mathbf{q}^r(hT + \tau)}^{-1} \mathbf{A}_{\mathbf{q}^r(hT + \tau)} - \mathbf{I}) \dot{\mathbf{q}}^r(hT + \tau) \\ &\stackrel{\text{def}}{=} \mathbf{f}(\mathbf{e}(hT + \tau), \mathbf{q}^r(hT + \tau), \dot{\mathbf{q}}^r(hT + \tau)). \end{aligned} \quad (14)$$

Proposition 2 *Under control strategy (13) the reference trajectory $\mathbf{q}^r(t)$ is an equilibrium trajectory, i.e.,*

$$\mathbf{q}(t) = \mathbf{q}^r(t) \Rightarrow \dot{\mathbf{e}}(t) = 0, \forall t \geq 0.$$

² $\dot{\mathbf{q}}^r(hT + \tau)$ is assumed to be continuously available at each controller since it has previously been computed by the global trajectory planner and deployed to the robots.

PROOF. If $\mathbf{q}(t) = \mathbf{q}^r(t)$, then $\mathbf{e}(t) \equiv 0$ and

$$\dot{\mathbf{e}}(hT + \tau) = (\mathbf{A}_{\mathbf{q}^r(hT + \tau)}^{-1} \mathbf{A}_{\mathbf{q}^r(hT + \tau)} - \mathbf{I}) \dot{\mathbf{q}}^r(hT + \tau) \equiv 0. \quad \square$$

Notice that, in virtue of the assumed structure (3) of the Jacobian $\mathbf{A}_{\mathbf{q}}$, the controller (13) can be decoupled across the robots, and is thus amenable of the sought decentralized implementation (6):

$$\begin{aligned} \mathbf{u}_i(hT + \tau) &= -k\mathbf{A}_{\mathbf{q}_i(hT)}^{(i)} (\mathbf{q}_i(hT) - \mathbf{q}_i^r(hT)) \\ &- k\mathbf{A}_{\mathbf{q}_V(hT)}^{(i)} (\mathbf{q}_V(hT) - \mathbf{q}_V^r(hT)) \\ &+ \mathbf{A}_{\mathbf{q}_i^r(hT + \tau)}^{(i)} \dot{\mathbf{q}}_i^r(hT + \tau) \\ &+ \mathbf{A}_{\mathbf{q}_V^r(hT + \tau)}^{(i)} \dot{\mathbf{q}}_V^r(hT + \tau). \end{aligned} \quad (15)$$

Proposition 2 implies that, if the initial configuration belongs to the reference trajectory, the control law (13) provides perfect tracking. However, this does not guarantee perfect (asymptotic) tracking starting from outside the reference trajectory, nor does it give conditions to asymptotic stability in terms of sampling period T and feedback gain k .

In the rest of this section, we will show that indeed the controller (13) does guarantee perfect asymptotic tracking for some values of (k, T) , and to this aim we study system (14). The flow $\mathbf{f}(\cdot, \cdot, \cdot)$ is discontinuous because the feedback term depends on $\mathbf{e}(hT)$, and resets at every sampling time $t = hT$. Thus, existence of a global solution based on standard Lipschitz continuity cannot be invoked, in general. However, in view of Assumption 1, the flow is Lipschitz continuous for $\tau \in [0, T)$. Hence, if we can show that a solution $\mathbf{e}(hT + \tau)$ exists for any $\tau \in [0, T)$, and that the limit $\lim_{\tau \rightarrow T} \mathbf{e}(hT + \tau)$ exists finite starting from any $\mathbf{e}(hT)$ satisfying Assumption 1, then global existence is guaranteed by patching together those intervals. As so, we study the flow $\mathbf{f}(\mathbf{e}(t), \mathbf{q}^r(t), \dot{\mathbf{q}}^r(t); \mathbf{e}(hT))$ for $t = hT + \tau$, $\tau \in [0, T)$, where we add the dependence on the “initial” condition $\mathbf{e}(hT)$. To prove asymptotic stability, we will use the following notion of contraction.

Definition 3 *Given fixed T, k , and under Assumption 1, the flow $\mathbf{f}(\mathbf{e}(t), \mathbf{q}^r(t), \dot{\mathbf{q}}^r(t); \mathbf{e}(hT))$ is ρ -monotonically contractive if, for any $\|\mathbf{e}(hT)\| < d$, it holds*

- (1) $\|\mathbf{e}(hT + \tau)\| \leq \|\mathbf{e}(hT)\|$, $\tau \in [0, T)$,
- (2) $\lim_{\tau \rightarrow T} \|\mathbf{e}(hT + \tau)\| \leq \rho \|\mathbf{e}(hT)\|$, $\rho \in [0, 1)$.

Given Definition 3, the following lemma easily follows.

Lemma 4 *If the error flow defined in (14) is ρ -monotonically contractive and under Assumption 1, then*

$$\|\mathbf{q}(t) - \mathbf{q}^r(t)\| \leq \rho^{\frac{t}{T} - 1} \|\mathbf{q}(0) - \mathbf{q}^r(0)\|, \quad t \geq 0.$$

Lemma 4 guarantees exponential convergence of the system trajectory to the reference. The property of ρ -monotonically contractiveness is rather strong since it must hold for any segment of the trajectory of length T , however, it allows proving asymptotic convergence. We first give a negative result in terms of ρ -monotonically contractiveness, which implies that the proposed controller may not work with an arbitrary choice of k .

Proposition 5 *Under Assumption 1, there exists $k_1 > 0$ such that, if one of the following conditions is satisfied,*

- (1) $k < k_1$,
- (2) $k > \frac{2}{T}$,

the error flow (14) is not ρ -monotonically contractive.

Intuitively, if the gain k is too small, there exist reference trajectories such that the feedforward term “pushes” the system too much without being suitably balanced by the feedback term. Conversely, if k is too large, the feedback causes the trajectory to overshoot, possibly amplifying the error of the initial condition.

PROOF. 1) We will prove the first condition showing that the error norm initially increases for some initial conditions $\mathbf{e}(hT)$ and choice of reference trajectory $\mathbf{q}^r(t)$. Consider the following Lyapunov function

$$V(\tau) = \frac{1}{2} \|\mathbf{e}(hT + \tau)\|^2, \quad (16)$$

and its time derivative at $\tau = 0$ (cf. (14)):

$$\begin{aligned} \dot{V}(0) &= \mathbf{e}(hT)^\top \dot{\mathbf{e}}(hT) \\ &= -k \|\mathbf{e}(hT)\|^2 + \\ &\quad \underbrace{\mathbf{e}^\top(hT) (\mathbf{A}_{\mathbf{e}(hT) + \mathbf{q}^r(hT)}^{-1} \mathbf{A}_{\mathbf{q}^r(hT)} - \mathbf{I}) \dot{\mathbf{q}}^r(hT)}_{\stackrel{\text{def}}{=} \phi(\mathbf{e}(hT), \mathbf{q}^r(hT), \dot{\mathbf{q}}^r(hT))}. \end{aligned}$$

Let us define

$$a \stackrel{\text{def}}{=} \max_{\substack{\|\mathbf{e}(hT)\| \leq d \\ \mathbf{q}^r(hT) \in \mathcal{Q} \\ \|\dot{\mathbf{q}}^r(hT)\| \leq v_{\max}}} \phi(\mathbf{e}(hT), \mathbf{q}^r(hT), \dot{\mathbf{q}}^r(hT)) \geq \alpha \|\mathbf{e}(hT)\|^2 v_{\max}$$

where the last inequality is valid for some $\alpha > 0$ and arises from the fact that all arguments of $\phi(\cdot)$ are defined on a compact set and that $\phi(\cdot)$ is continuously differentiable. The only case for which the inequality is not satisfied is when $\mathbf{A}_{\mathbf{q}}$ is a constant matrix for all \mathbf{q} which is clearly false. This implies that there exist tuples $(\mathbf{e}(hT), \mathbf{q}^r(hT), \dot{\mathbf{q}}^r(hT))$ such that

$$\dot{V}(0) \geq -(k - \alpha v_{\max}) \|\mathbf{e}(hT)\|^2.$$

Let $k_1 \stackrel{\text{def}}{=} \alpha v_{\max}$, then $\dot{V}(0) > 0$ for any $k < k_1$, hence there exists $0 < \bar{\tau} < T$ s.t. $\|\mathbf{e}(hT + \tau)\| > \|\mathbf{e}(hT)\| \forall \tau \in (0, \bar{\tau})$ and (14) it is not ρ -monotonically contractive.

2) In order to prove the second condition we first choose $\mathbf{q}^r(t) \equiv \mathbf{q}^r$, $t \geq 0$, which satisfies Assumption 1. As so, the error dynamics reduce to

$$\dot{\mathbf{e}}(hT + \tau) = -k \underbrace{\mathbf{A}_{\mathbf{e}(hT + \tau) + \mathbf{q}^r}^{-1} \mathbf{A}_{\mathbf{e}(hT) + \mathbf{q}^r}}_{\stackrel{\text{def}}{=} \mathbf{g}(\mathbf{e}(hT + \tau))} \mathbf{e}(hT).$$

The error trajectory can be written in the form

$$\mathbf{e}(hT + \tau) = \mathbf{e}(hT) + k \int_{hT}^{hT + \tau} \mathbf{g}(\mathbf{e}(hT + \tau')) d\tau'.$$

By using Taylor's theorem for multivariate functions with integral form of the remainder, it becomes

$$\begin{aligned} \mathbf{e}(hT + \tau) &= \mathbf{e}(hT) + k\tau \mathbf{g}(\mathbf{e}(hT)) + \\ &+ k^2 \tau^2 \int_0^1 (1 - \varepsilon) \frac{\partial \mathbf{g}(\mathbf{e}(hT + \varepsilon\tau))}{\partial \mathbf{e}} \mathbf{g}(\mathbf{e}(hT + \varepsilon\tau)) d\varepsilon \\ &= (1 - k\tau) \mathbf{e}(hT) + k^2 \tau^2 \mathbf{r}(\mathbf{e}(hT + \tau); \mathbf{e}(hT)), \end{aligned} \quad (17)$$

where $\mathbf{r}(\cdot)$ is the second-order reminder where we made explicit the dependence on $\mathbf{e}(hT)$. Under Assumption 1, the functions \mathbf{g} and $\frac{\partial \mathbf{g}}{\partial \mathbf{e}}$ are continuously differentiable. Moreover their arguments are defined in a compact set and have the additional properties that $\mathbf{g}(\mathbf{e}(hT + \tau)) = 0$, $\frac{\partial \mathbf{g}(hT + \tau)}{\partial \mathbf{e}} = \mathbf{0}$, $\forall \tau \in [0, T]$ if $\mathbf{e}(hT) = \mathbf{0}$. Therefore, applying Lemma A.3, there must exist $\delta > 0$ such that

$$\|\mathbf{r}(\mathbf{e}(hT + \tau); \mathbf{e}(hT))\| \leq \delta \|\mathbf{e}(hT)\|^2, \quad \forall \tau \in [0, T], \forall \mathbf{e}(hT).$$

We now use the reverse triangle inequality and the previous inequality to get:

$$\begin{aligned} \|\mathbf{e}(hT + \tau)\| &\geq \\ &\geq \|(1 - k\tau) \mathbf{e}(hT)\| - k^2 \tau^2 \|\mathbf{r}(\mathbf{e}(hT + \tau); \mathbf{e}(hT))\| \\ &\geq \max\{0, |1 - k\tau| - k^2 \tau^2 \delta \|\mathbf{e}(hT)\|\} \|\mathbf{e}(hT)\|. \end{aligned} \quad (18)$$

If $kT > 2$, there exist $\epsilon > 0$ and $\bar{\tau} \in (0, T)$ s.t. $k\bar{\tau} = 2 + \epsilon$. Then, we can choose $\mathbf{e}(hT)$ s.t. $\|\mathbf{e}(hT)\| = \frac{\epsilon}{2k\bar{\tau}^2\delta}$, hence

$$\|\mathbf{e}(hT + \bar{\tau})\| \geq \left(1 + \epsilon - \frac{\epsilon}{2}\right) \|\mathbf{e}(hT)\| \geq \|\mathbf{e}(hT)\|. \quad \square$$

Proposition 5 states that there are choices of T and k for which the error flow is not ρ -monotonically contractive. However, there exist pairs of T and k for which ρ -monotonically contractiveness holds.

Proposition 6 *Under Assumption 1, there exists $k_2 > 0$ such that for any $k > k_2$ there exists $T_c(k)$ such that for all $T < T_c(k)$ the error flow defined in (14) is ρ -monotonically contractive.*

PROOF. Consider the Lyapunov function (16) and its time derivative at $\tau = 0$:

$$\begin{aligned} \dot{V}(0) &= -k\|\mathbf{e}(hT)\|^2 + \\ &+ \mathbf{e}^\top(hT)(\mathbf{A}_{\mathbf{e}(hT)+\mathbf{q}^r(hT)}^{-1}\mathbf{A}_{\mathbf{q}^r(hT)} - \mathbf{I})\dot{\mathbf{q}}^r(hT). \end{aligned}$$

Note that $\mathbf{A}_{\mathbf{e}(hT)+\mathbf{q}^r(hT)}^{-1}\mathbf{A}_{\mathbf{q}^r(hT)} - \mathbf{I} = \mathbf{0} \ \forall \mathbf{q}^r(hT)$ if $\mathbf{e}(hT) = \mathbf{0}$. Moreover, being $\mathbf{e}(hT)$ and $\mathbf{q}^r(hT)$ in a compact set according to Assumption 1, it holds $\|\mathbf{A}_{\mathbf{e}(hT)+\mathbf{q}^r(hT)}^{-1}\mathbf{A}_{\mathbf{q}^r(hT)} - \mathbf{I}\| \leq \delta\|\mathbf{e}(hT)\|$ for some $\delta > 0$, therefore

$$\begin{aligned} \dot{V}(0) &\leq -k\|\mathbf{e}(hT)\|^2 + \delta\|\mathbf{e}(hT)\|^2 v_{max} \\ &= -(k - \delta v_{max})\|\mathbf{e}(hT)\|^2 = -2(k - \delta v_{max})V(0). \end{aligned}$$

Let $k_2 \stackrel{\text{def}}{=} \delta v_{max}$, then for each $k > k_2$, there exist $\xi \in (0, k - \delta v_{max})$ and $T_c(k)$ s.t.

$$\begin{aligned} V(\tau) &\leq e^{-2\xi\tau}V(0), \tau \in [0, T_c(k)) \\ \implies \|\mathbf{e}(hT + \tau)\| &\leq e^{-\xi\tau}\|\mathbf{e}(hT)\|, \tau \in [0, T_c(k)). \end{aligned}$$

As a consequence, by defining $\rho \stackrel{\text{def}}{=} e^{-T\xi} < 1$ for any $T < T_c(k)$, it holds

$$\begin{aligned} \|\mathbf{e}(hT + \tau)\| &\leq \rho\|\mathbf{e}(hT)\|, \tau \in [0, T) \\ \lim_{\tau \rightarrow T} \|\mathbf{e}(hT + \tau)\| &\leq \rho\|\mathbf{e}(hT)\|, \end{aligned}$$

i.e., the system is ρ -monotonically contractive. \square

By combining this result with the previous one, it follows that $\lim_{k \rightarrow \infty} T_c(k) = 0$ and that there exists $T_{max} > 0$ such that $T_c(k) < T_{max}, \forall k > k_2$. Such quantities are depicted in Fig. 1. From Proposition 5, we know that the error flow (14) is not ρ -monotonically contractive for values of (k, T) in the red area. Conversely, the curve $T_c(k)$ introduced in Proposition 6 bounds the area where the flow (14) is ρ -monotonically contractive. In the next section, we show how to obtain an estimate of $T_c(k)$. Since our analysis is based on upper bounds on the tracking error norm, we provide the underestimate $\tau_s(k)$.

4 Stability and Convergence Rate Bounds

All results in the previous section are of existential type, i.e., they give no indication about computing the pairs k and T for which the system is ρ -monotonically contractive, nor the convergence rate ρ . In this section, we

find explicit bounds on the “stability” set (green area in Fig. 1) where the error norm decreases. Also, we characterize the convergence rate and find the pairs of gain and sampling time that induce the fastest convergence.

Remark 7 (Stability) *When mentioning stability, we imply that the flow (14) is ρ -monotonically contractive.*

Proposition 8 *For system (14), it is possible to upper bound the decrease rate of the error norm $\|\mathbf{e}(\cdot)\|$,*

$$\|\mathbf{e}(hT + \tau)\| \leq z(k, \tau; \mu, \alpha, \gamma_1, \gamma_2) \cdot \|\mathbf{e}(hT)\|, \quad (19)$$

for $h \in \mathbb{N}$, $\tau \in (0, \tau_s(k))$, and

$$z(k, \tau; \mu, \alpha, \gamma_1, \gamma_2) = |1 - k\tau| + \tau\alpha + \tau^2(k^2\mu + k\gamma_1 + \gamma_2),$$

where $\alpha, \mu, \gamma_1, \gamma_2$ are positive constants.

PROOF. [Sketch] In virtue of the Lipschitz properties of the error flow in the interval $(hT, hT + T)$, Taylor’s theorem with integral form of the remainder for multivariate functions is used to decompose the error $\mathbf{e}(hT + \tau)$ as a sum of terms which can be upper bounded individually. Notice that α, μ, γ_1 and γ_2 are still unknown at this stage.

PROOF. The flow defined by (14) can be written as

$$\mathbf{e}(hT + \tau) = \mathbf{e}(hT) + \int_{hT}^{hT + \tau} \mathbf{f}(\mathbf{e}(\cdot), \mathbf{q}^r(\cdot), \dot{\mathbf{q}}^r(\cdot)) \Big|_{hT + \tau'} d\tau'.$$

By using Taylor’s theorem for multivariate functions with integral form of the remainder, we get

$$\begin{aligned} \mathbf{e}(hT + \tau) &= \mathbf{e}(hT) + \tau \mathbf{f}(\mathbf{e}(hT), \mathbf{q}^r(hT), \dot{\mathbf{q}}^r(hT)) + \\ &+ \tau^2 \int_0^1 (1 - \varepsilon) \cdot \left[\frac{\partial \mathbf{f}(\mathbf{e}(\cdot), \mathbf{q}^r(\cdot), \dot{\mathbf{q}}^r(\cdot))}{\partial \mathbf{e}(\cdot)} \mathbf{f}(\mathbf{e}(\cdot), \mathbf{q}^r(\cdot), \dot{\mathbf{q}}^r(\cdot)) + \right. \\ &+ \frac{\partial \mathbf{f}(\mathbf{e}(\cdot), \mathbf{q}^r(\cdot), \dot{\mathbf{q}}^r(\cdot))}{\partial \mathbf{q}^r(\cdot)} \dot{\mathbf{q}}^r(\cdot) + \\ &\left. + \frac{\partial \mathbf{f}(\mathbf{e}(\cdot), \mathbf{q}^r(\cdot), \dot{\mathbf{q}}^r(\cdot))}{\partial \dot{\mathbf{q}}^r(\cdot)} \ddot{\mathbf{q}}^r(\cdot) \right]_{hT + \varepsilon\tau} d\varepsilon. \end{aligned} \quad (20)$$

The above expression allows to find an upper bound of $\|\mathbf{e}(hT + \tau)\|$, $\tau \in (0, \tau_s(k))$, by acting on the single terms of (20). Hence, we can compute a more precise estimate of the convergence rate, i.e., how quickly $\|\mathbf{e}(hT + \tau)\|$, with $\tau \in (0, \tau_s(k))$, decreases w.r.t. $\|\mathbf{e}(hT)\|$. Moreover, the following computations will be useful to find values (k, T) s.t. the system is stable and the tracking error converges to zero. First, we observe that

$$\begin{aligned} \mathbf{f}(\mathbf{e}(hT), \mathbf{q}^r(hT), \dot{\mathbf{q}}^r(hT)) &= -k\mathbf{e}(hT) + \\ &+ (\mathbf{A}_{\mathbf{e}(hT)+\mathbf{q}^r(hT)}^{-1}\mathbf{A}_{\mathbf{q}^r(hT)} - \mathbf{I}) \dot{\mathbf{q}}^r(hT). \end{aligned} \quad (21)$$

By using Lemma A.2 on the second addend, it holds

$$\|(\mathbf{A}_{\mathbf{e}(hT)+\mathbf{q}^r(hT)}^{-1}\mathbf{A}_{\mathbf{q}^r(hT)} - \mathbf{I})\dot{\mathbf{q}}^r(hT)\| \leq \alpha\|\mathbf{e}(hT)\|,$$

where $\alpha \stackrel{\text{def}}{=} av_{max}$. Moreover, from (14),

$$\begin{aligned} & \|\mathbf{f}(\mathbf{e}(hT+\tau), \mathbf{q}^r(hT+\tau), \dot{\mathbf{q}}^r(hT+\tau))\| \leq \\ & \leq \| -k\mathbf{A}_{\mathbf{e}(hT+\tau)+\mathbf{q}^r(hT+\tau)}^{-1}\mathbf{A}_{\mathbf{e}(hT)+\mathbf{q}^r(hT)}\mathbf{e}(hT)\| + \\ & + \|(\mathbf{A}_{\mathbf{e}(hT+\tau)+\mathbf{q}^r(hT+\tau)}^{-1}\mathbf{A}_{\mathbf{q}^r(hT+\tau)} - \mathbf{I})\dot{\mathbf{q}}^r(hT+\tau)\|. \end{aligned} \quad (22)$$

Both addends in (22) are continuously differentiable functions on a compact set. In addition, they are equal to zero if $\mathbf{e}(hT) = \mathbf{0}$ and $\mathbf{e}(hT+\tau) = \mathbf{0}$, respectively. Then, we can apply Lemmas A.1-A.2 to get $\|k\mathbf{A}_{\mathbf{e}(hT+\tau)+\mathbf{q}^r(hT+\tau)}^{-1}\mathbf{A}_{\mathbf{e}(hT)+\mathbf{q}^r(hT)}\mathbf{e}(hT)\| \leq kb\|\mathbf{e}(hT)\|$, $b > 0$, and $\|(\mathbf{A}_{\mathbf{e}(hT+\tau)+\mathbf{q}^r(hT+\tau)}^{-1}\mathbf{A}_{\mathbf{q}^r(hT+\tau)} - \mathbf{I})\dot{\mathbf{q}}^r(hT+\tau)\| \leq c\|\mathbf{e}(hT)\|v_{max}$, $c > 0$, where we used Proposition 6 and Definition 3. Thus, we rewrite (22) as

$$\|\mathbf{f}(\mathbf{e}(\cdot), \mathbf{q}^r(\cdot), \dot{\mathbf{q}}^r(\cdot))\|_{hT+\tau} \leq (kb+cv_{max})\|\mathbf{e}(hT)\|. \quad (23)$$

Also, being $\mathbf{f}(\mathbf{e}(\cdot), \mathbf{q}^r(\cdot), \dot{\mathbf{q}}^r(\cdot))$ differentiable w.r.t. all its variables on the compact set $\mathcal{B}_r(\mathbf{e}(\cdot))$, we can derive the following bounds based on (21) :

$$\begin{aligned} & \left\| \frac{\partial \mathbf{f}(\mathbf{e}(\cdot), \mathbf{q}^r(\cdot), \dot{\mathbf{q}}^r(\cdot))}{\partial \mathbf{e}} \right\|_{hT+\tau} \leq (k+gv_{max})\|\mathbf{e}(hT)\| \\ & \left\| \frac{\partial \mathbf{f}(\mathbf{e}(\cdot), \mathbf{q}^r(\cdot), \dot{\mathbf{q}}^r(\cdot))}{\partial \mathbf{q}^r} \right\|_{hT+\tau} \leq mv_{max}\|\mathbf{e}(hT)\| \\ & \left\| \frac{\partial \mathbf{f}(\mathbf{e}(\cdot), \mathbf{q}^r(\cdot), \dot{\mathbf{q}}^r(\cdot))}{\partial \dot{\mathbf{q}}^r} \right\|_{hT+\tau} \leq kn\|\mathbf{e}(hT)\|, \end{aligned} \quad (24)$$

where $g, m, n > 0$. In virtue of (21), (23) and (24), we can derive the overall bound defined in (19):

$$\|\mathbf{e}(hT+\tau)\| \leq (|1-k\tau| + \alpha\tau + \tau^2(k^2\mu + k\gamma_1 + \gamma_2))\|\mathbf{e}(hT)\|$$

where, given $a > 0$ defined in the proof of Proposition 5,

$$\begin{aligned} \alpha & \stackrel{\text{def}}{=} av_{max} \\ \mu & \stackrel{\text{def}}{=} b\|\mathbf{e}(hT)\| \\ \gamma_1 & \stackrel{\text{def}}{=} (c+gb)v_{max}\|\mathbf{e}(hT)\| + na_{max} \\ \gamma_2 & \stackrel{\text{def}}{=} gc v_{max}\|\mathbf{e}(hT)\| + m v_{max}. \quad \square \end{aligned}$$

Proposition 8 provides an expression for the convergence rate as a function of the parameters $\mu, \alpha, \gamma_1, \gamma_2$. In the next section, we provide a procedure to estimate them.

4.1 Estimating the Parameters $\mu, \alpha, \gamma_1, \gamma_2$

We would like to find an estimate of the function $z(k, \tau; \mu, \alpha, \gamma_1, \gamma_2)$ that bounds the convergence rate of the tracking error, and choose the values (k, T) which yield the fastest convergence. To this aim, we provide a numerical procedure to estimate $\theta \stackrel{\text{def}}{=} (\mu, \alpha, \gamma_1, \gamma_2)$. Proposition 8 implies that the following set is not empty:

$$\Theta \stackrel{\text{def}}{=} \{\theta > 0 \mid \|\mathbf{e}(hT+\tau)\| \leq z(k, \tau; \theta)\|\mathbf{e}(hT)\|, \forall \mathbf{q}^r(\cdot), \mathbf{q}(0)\}$$

where the inequality is componentwise. Ideally, we would like to pick the smallest possible values for the parameters in θ in order to get the largest set of pairs (k, T) that induce stability. One possibility is choosing

$$\vartheta \stackrel{\text{def}}{=} \underset{\theta \in \Theta}{\operatorname{argmin}} \|\theta\|.$$

Such ϑ surely exists because $\mathbf{q}^r(\cdot)$ and $\mathbf{q}(0)$ belong to a compact set. However, it cannot be computed numerically because one would need to check all pairs (k, T) and points $\mathbf{q}^r(t)$ and $\mathbf{q}(0)$. We propose a strategy to estimate ϑ by sampling $\mathbf{q}^r(t)$ and $\mathbf{q}(0)$ from their domains for different values of (k, T) and run simulations to get a set of samples $\{(k_i, T_i, \mathbf{e}_{h+1}^i, \mathbf{e}_h^i)\}_{i=1}^S$, S being the number of samples. Let us define the following quantities:

$$\begin{aligned} y_i & \stackrel{\text{def}}{=} \|\mathbf{e}_{h+1}^i\|, \\ a_i^T & \stackrel{\text{def}}{=} [T_i^2 \ k_i^2 \ T_i \ T_i^2 k_i \ T_i^2] \|\mathbf{e}_h^i\| \\ b_i & \stackrel{\text{def}}{=} |1 - k_i T_i| \|\mathbf{e}_h^i\|. \end{aligned}$$

then the inequality $\|\mathbf{e}_{h+1}^i\| \leq z(k_i, T_i; \theta)\|\mathbf{e}_h^i\|$ can be written as $y_i \leq a_i^T \theta + b_i$. Based on such sampled trajectories, we solve the following quadratic programming:

$$\begin{aligned} \hat{\theta}_S & \stackrel{\text{def}}{=} \underset{\theta}{\operatorname{argmin}} \|\theta\|^2 \\ \text{s. t.} \quad & \theta \geq 0, \\ & y_i \leq A_i \theta + b_i, \quad i = 1, \dots, S. \end{aligned} \quad (25)$$

Unfortunately, it is possible that $\hat{\theta}_S \notin \Theta$ since we are checking the inequality $\|\mathbf{e}(hT+\tau)\| \leq z(k, \tau; \theta)\|\mathbf{e}(hT)\|$ over a finite number of points. We expect that $\lim_{S \rightarrow \infty} \hat{\theta}_S = \vartheta$ if we sample different enough $\mathbf{q}^r(\cdot)$ and $\mathbf{q}(0)$. However, a formal proof of this claim is not trivial. There might be alternative numerical strategies to compute better estimates of ϑ , or alternative parameter choices in the set Θ . Such comparison goes beyond the scope of this work, however, we will show through simulations that our proposed strategy is indeed effective.

4.2 Analysis of the Function $z(k, \tau; \mu, \alpha, \gamma_1, \gamma_2)$

In this section, we analyze the function $z(k, \tau; \mu, \alpha, \gamma_1, \gamma_2)$ in order to compute the convergence rate of the error and to bound the stability region (green area in Fig. 1), i.e., where $z(k, \tau; \mu, \alpha, \gamma_1, \gamma_2) < 1$. We also compute the optimal controller gain $k_o(T)$ for a fixed sampling time T and the optimal sampling time $T_s(k)$ for a fixed gain k to achieve the fastest convergence rate. Notice that $z(k, \tau; \mu, \alpha, \gamma_1, \gamma_2)$ can be written as³:

$$z(k, \tau) = \begin{cases} z^-(k, \tau) & \text{if } k\tau < 1 \\ z^+(k, \tau) & \text{if } k\tau > 1 \end{cases},$$

where

$$\begin{aligned} z^-(k, \tau) &= 1 + \tau(\alpha - k) + \tau^2(k^2\mu + k\gamma_1 + \gamma_2) \\ z^+(k, \tau) &= -1 + \tau(\alpha + k) + \tau^2(k^2\mu + k\gamma_1 + \gamma_2). \end{aligned}$$

We aim to find the stability set defined as

$$\mathcal{U} \stackrel{\text{def}}{=} \{(k, \tau) | z(k, \tau) < 1\}.$$

Proposition 9 *The stability set of $z(k, \tau)$ is*

$$\mathcal{U} = \{\alpha < k < +\infty, 0 < \tau < \tau_s(k)\},$$

where $\alpha = k_{\min}$ was defined in Proposition 8 and

$$\tau_s(k) = \begin{cases} \tau_{s_1}(k) & \alpha < k < \bar{k} \text{ if } \mu > 1 \\ \tau_{s_1}(k) & \alpha < k < \bar{k} \text{ if } \mu < 1, \\ \tau_{s_2}(k) & k > \bar{k} \text{ if } \mu < 1 \end{cases}$$

$$\begin{aligned} \text{where } \tau_{s_1} &\stackrel{\text{def}}{=} \frac{k-\alpha}{k^2\mu+k\gamma_1+\gamma_2}, \bar{k} \stackrel{\text{def}}{=} \frac{\alpha+\gamma_1+\sqrt{(\alpha+\gamma_1)^2+4\gamma_2(1-\mu)}}{2(1-\mu)}, \\ \tau_{s_2} &\stackrel{\text{def}}{=} \frac{-(\alpha+k)+\sqrt{(\alpha+k)^2+8(k^2\mu+k\gamma_1+\gamma_2)}}{2(k^2\mu+k\gamma_1+\gamma_2)}. \end{aligned}$$

With fixed k , we can define the sampling time and convergence rate as functions of k :

$$\tau_o(k) \stackrel{\text{def}}{=} \underset{\tau}{\operatorname{argmin}} z(k, \tau) \quad (26)$$

$$\rho_o(k) \stackrel{\text{def}}{=} z(k, \tau_o(k)), \quad (27)$$

where τ_o is the time when $\|e(hT + \tau)\|$, $0 \leq \tau \leq T$, is closest to the origin, hence it corresponds to the fastest convergence rate of the error ρ_o .

³ In the following, we use the shorthand notation $z(k, \tau) \stackrel{\text{def}}{=} z(k, \tau; \mu, \alpha, \gamma_1, \gamma_2)$ for the sake of readability.

Proposition 10 *With fixed k , the optimal sampling time $\tau_o(k)$ is given by*

$$\tau_o(k) = \begin{cases} \tau_{o_1}(k) & \text{for } \alpha < k < \bar{k} \text{ if } \mu > \frac{1}{2} \\ \tau_{o_1}(k) & \text{for } \alpha < k < \bar{k} \text{ if } \mu < \frac{1}{2}, \\ \frac{1}{k} & \text{for } k > \bar{k} \text{ if } \mu < \frac{1}{2} \end{cases}$$

$$\tau_{o_1}(k) \stackrel{\text{def}}{=} \frac{k-\alpha}{2(k^2\mu+k\gamma_1+\gamma_2)}, \bar{k} \stackrel{\text{def}}{=} \frac{\alpha+2\gamma_1+\sqrt{(\alpha+2\gamma_1)^2+8\gamma_2(1-2\mu)}}{2(1-2\mu)}.$$

The corresponding convergence rate $\rho_o(k)$ is

$$\rho_o(k) = \begin{cases} \rho_{k_1}(k) & \text{if } \mu > \frac{1}{2} \\ \rho_{k_1}(k) & \text{for } \alpha < k < \bar{k} \text{ if } \mu < \frac{1}{2}, \\ \rho_{k_2}(k) & \text{for } k > \bar{k} \text{ if } \mu < \frac{1}{2} \end{cases}$$

where $\rho_{k_1}(k) \stackrel{\text{def}}{=} 1 - \frac{(\alpha-k)^2}{4(k^2\mu+k\gamma_1+\gamma_2)}$ and $\rho_{k_2}(k) \stackrel{\text{def}}{=} \mu + \frac{1}{k}(\alpha + \gamma_1) + \frac{\gamma_2}{k^2}$.

The same quantities can be found as functions of τ :

$$k_o(\tau) \stackrel{\text{def}}{=} \underset{k}{\operatorname{argmin}} z(k, \tau) \quad (28)$$

$$\rho_o(\tau) \stackrel{\text{def}}{=} z(k_o(\tau), \tau). \quad (29)$$

Proposition 11 *With fixed τ , the optimal gain $k_o(\tau)$ is given by*

$$k_o(\tau) = \begin{cases} \frac{1-\tau\gamma_1}{2\tau\mu} & \text{for } \tau < \frac{1}{\gamma_1} \text{ if } \mu > \frac{1}{2} \\ \frac{1-\tau\gamma_1}{2\tau\mu} & \text{for } \tau_{m_k} < \tau < \tau_{M_k} \text{ if } \mu < \frac{1}{2}, \\ \frac{1}{\tau} & \text{for } 0 < \tau < \tau_{m_k} \text{ if } \mu < \frac{1}{2} \end{cases}$$

where $\tau_{m_k} \stackrel{\text{def}}{=} \frac{1-2\mu}{\gamma_1}$, $\tau_{M_k} \stackrel{\text{def}}{=} \frac{1}{\gamma_1}$. The corresponding convergence rate $\rho_o(\tau)$ is:

$$\rho_o(\tau) = \begin{cases} \rho_{\tau_1}(\tau) & \text{for } \tau < \tau_{v_2}^- \text{ if } \mu > \frac{1}{2} \\ \rho_{\tau_1}(\tau) & \text{for } \tau_{m_\tau} < \tau < \tau_{M_\tau} \text{ if } \mu < \frac{1}{2}, \\ \rho_{\tau_2}(\tau) & \text{for } 0 < \tau < \tau_{m_\tau} \text{ if } \mu < \frac{1}{2} \end{cases}$$

where $\rho_{\tau_1}(\tau) \stackrel{\text{def}}{=} \frac{(-\gamma_1^2+4\gamma_2\mu)\tau^2+2(\gamma_1+2\alpha\mu)\tau+4\mu-1}{4\mu}$, $\rho_{\tau_2}(\tau) \stackrel{\text{def}}{=} \gamma_2\tau^2 + (\alpha + \gamma_1)\tau + \mu$, $\tau_{m_\tau} \stackrel{\text{def}}{=} \min\{\frac{1-2\mu}{\gamma_1}, \tau_{v_2}^-\}$, $\tau_{M_\tau} \stackrel{\text{def}}{=} \max\{\frac{1-2\mu}{\gamma_1}, \tau_{v_2}^-\}$, and $\tau_{v_2}^- = \frac{-(\gamma_1+\alpha\mu)+\sqrt{(\gamma_1+\alpha\mu)^2+(-\gamma_1^2+4\gamma_2\mu)}}{-\gamma_1^2+4\gamma_2\mu}$.

The proofs of Propositions 9–11 are provided in Appendix C.

Figure 5 depicts the quantities defined above: in particular, $\tau(k_o)$ is obtained by inverting $k_o(\tau)$, being this

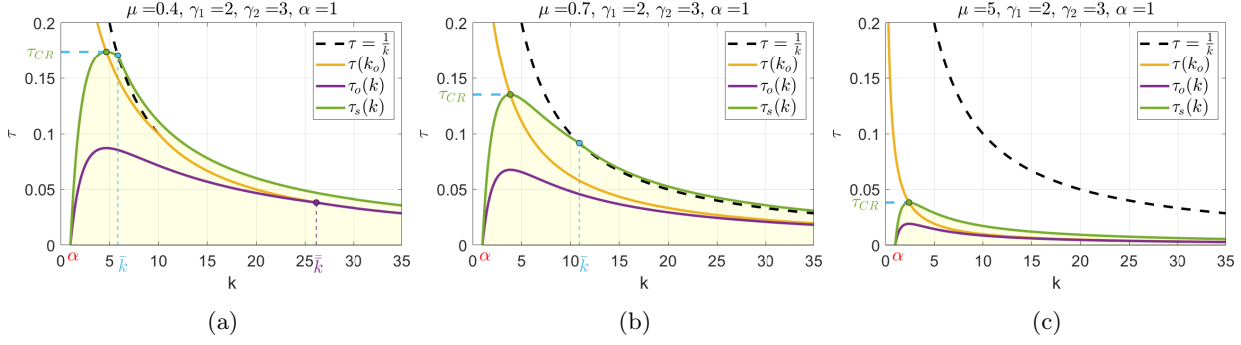


Fig. 5. Representation of the quantities $\tau_s(k)$, $\tau_o(k)$, $\tau(k_o)$ defined in Propositions 9–11.

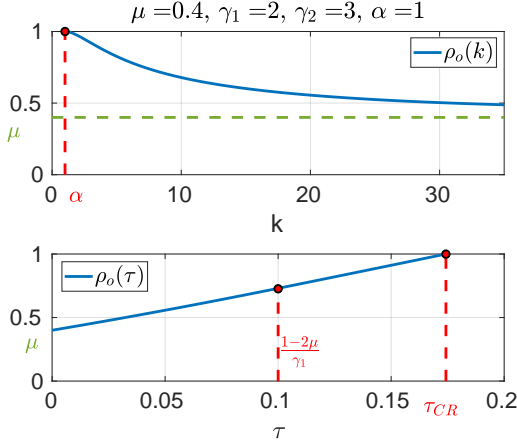


Fig. 6. Estimated convergence rate ρ_0 as a function of the gain k and of the sampling time τ .

monotonic decreasing, and represents the sampling time for which k_o is the optimal gain. We chose three cases corresponding to $\mu < 1/2$ (Fig. 5a), $1/2 < \mu < 1$ (Fig. 5b), and $\mu > 1$ (Fig. 5c), in order to span the cases given in the previous propositions. Note that $\tau = 1/k$ represents the value s.t. $z^-(k, \tau) = z^+(k, \tau)$. Figure 6 represents the convergence rate ρ_o as a function of k (top plot) and τ (bottom plot). The convergence rate is always smaller than one, hence $\|\mathbf{e}(hT + \tau)\| \leq \|\mathbf{e}(hT)\|$, $\tau \in [0, T]$.

Remark 12 (Constant reference) Consider (19) and suppose a constant reference is assigned, i.e., $\frac{d^{(n)}}{dt^{(n)}} \mathbf{q}^r(t) \equiv \mathbf{0}$, $n \geq 1$. Then $\alpha = \gamma_1 = \gamma_2 = 0$ and $z(k, \tau; \mu)$ coincides with the function $g(\tau; \mu)|_{\tau=k\tau}$ found in [21].

Remark 13 (Sampling time and stabilizability) There exists a critical sampling time τ_{CR} s.t. the system cannot be stabilized for any choice of the controller gain. Such a critical value can be used to evaluate the communication hardware to be used.

5 Simulation Results

In this section, we implement and compare four techniques for trajectory tracking, which are summarized in Table 1. PT is the point-stabilization control (11), where the gain $k = k_{\text{on}}$ is designed online following the strategy proposed in [21] (see Appendix D). In particular, at the h th step, k_{on} is the solution to the following optimization problem with initial condition $\mathbf{e}_h = \mathbf{e}(hT)$:

$$\begin{aligned} k_{\text{on}}(\mathbf{e}_h) = \underset{k}{\operatorname{argmin}} \quad & \|\mathbf{e}(hT + T)\| \\ \text{s. t.} \quad & (11). \end{aligned} \quad (30)$$

The online gain is computed similarly to the offline one, with the key difference that a sharper bound is obtained on the error convergence, and thus superior performance is achieved: indeed, the offline design solves the (more conservative) min-max version of (30) where the maximum is taken over h , optimizing over the worst segment of trajectory. However, the online gain computation has the drawback of requiring centralized implementation. FF implements the naive feedforward (12) where the Jacobian is evaluated at \mathbf{q}_{hT} , with the gain k_{on} computed online as in PT. SIKM-C implements the centralized control law (13) with the gain $k = k_{\text{on}}$ computed online, as this intuitively allows to reach faster convergence. SIKM-D is our final tracking solution, i.e. control (13) with the decentralized implementation (15), where the optimal gain $k = k_{\text{off}}$ is computed offline following the procedure in Sec. 4 with provable stability guarantees.

Remark 14 (Benefits of decentralized controller) We stress that our aim is not only to design a controller

Control Strategy	$\mathbf{u}_k(hT)$	$\mathbf{u}_h(hT + \tau)$
PT (Eq. (11))	$-k_{\text{on}} \mathbf{A}_{\mathbf{q}_h} (\mathbf{q}_h - \mathbf{q}_h^r)$	$\mathbf{0}$
FF (Eq. (12))	$-k_{\text{on}} \mathbf{A}_{\mathbf{q}_h} (\mathbf{q}_h - \mathbf{q}_h^r)$	$\mathbf{A}_{\mathbf{q}_{hT}} \dot{\mathbf{q}}_{hT+\tau}^r$
SIKM-C (Eq. (13))	$-k_{\text{on}} \mathbf{A}_{\mathbf{q}_h} (\mathbf{q}_h - \mathbf{q}_h^r)$	$\mathbf{A}_{\mathbf{q}_{hT+\tau}^r} \dot{\mathbf{q}}_{hT+\tau}^r$
SIKM-D (Eq. (15))	$-k_{\text{off}} \mathbf{A}_{\mathbf{q}_h} (\mathbf{q}_h - \mathbf{q}_h^r)$	$\mathbf{A}_{\mathbf{q}_{hT+\tau}^r} \dot{\mathbf{q}}_{hT+\tau}^r$

Table 1

Description of the four strategies used in simulation.

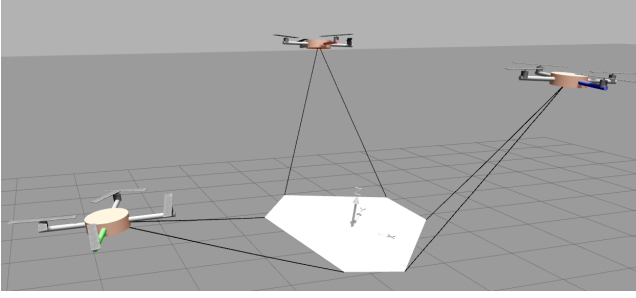


Fig. 7. The Fly-Crane system in the Gazebo simulator.

to make the multi-robot system track the desired trajectory, but also to allow for a decentralized implementation of such a controller. This avoids practical limitations due to centralized strategies, which are prone to communication non-idealities such as latency or packet loss caused by collisions, are less robust, more costly and complicated to maintain, and do not scale with the size of the system as for required communication overhead.

Remark 15 (Real-time computation of k_{on}) For PT control, the online gain optimization (30) can be performed exactly (up to numerical precision) while complying with real-time computational constraints. By contrast, the gain adaptation for FF and SIKM-C, with control dynamics given respectively by (12) and (13), cannot be performed in real time through the presence of the feedforward term. Therefore, the design (30) is used also in the latter two cases, in virtue of its theoretical guarantees for point-stabilization that intuitively carry over (to some extent) also with time-varying trajectories. Indeed, simulations show that both FF and SIKM-C perform well when the online gain is designed as per (30).

We simulate the four techniques on the *Fly-Crane* system [23], whose simulated environment is depicted in Fig. 7. The dynamical model of the system has been developed in a physics-based simulator (Gazebo), simulating cables dynamics as well. Simulations have been done with *software in the loop* simulating sensor noise and communication delays. Communication across the system, planning and sensing are implemented using a middle-ware called *Pocolibs* and the software framework *genoM*, resulting in very realistic simulations.

The used system architecture is represented in Fig. 8: a global planner generates offline the desired trajectory ($\mathbf{q}^r, \dot{\mathbf{q}}^r$) and this information is made available to the SIKM controller, implemented in Matlab-Simulink. The latter generates the desired robot velocities \mathbf{u}_i which are sent to the robots every T seconds via wireless. Then, the low-level dynamical controller (geometric position controller [13]) of each robot converts these velocities into thrust and torque for the quadrotors. An unscented Kalman filter, running at 1 [kHz], fuses the Motion Capture (MoCap) system measurements (at 120 [Hz]) with the IMU measurements (at 1 [kHz]). The estimated system state is then sent to the SIKM controller.

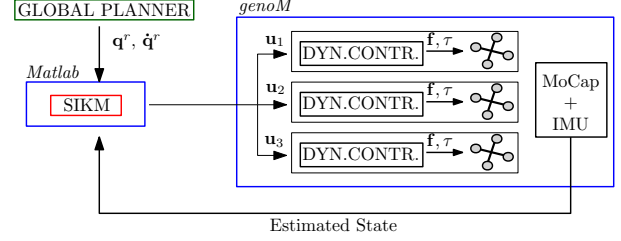


Fig. 8. Architecture used to perform simulations: a global planner generates the desired trajectory $\mathbf{q}^r, \dot{\mathbf{q}}^r$ and sends it to the local planner which generates the desired robot velocities. The blue rectangle on the right represents a realistic environment where the robotic system is simulated.

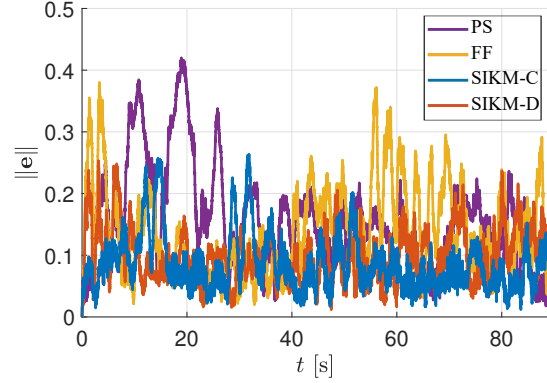


Fig. 9. Tracking error norm $\|\mathbf{e}(t)\| = \|\mathbf{q}(t) - \mathbf{q}^r(t)\|$ obtained with the tracking strategies described in Table 1 ($T = 1.5[s]$).

We first compare the tracking error norm for the four control strategies when $T = 1.5[s]$ (see Figs. 9 and 10). Notice that the tracking error does not converge to zero because of non-idealities implemented in simulation, as sensor noise. The desired trajectory was generated in order to stress all components of \mathbf{q} , except for y -translation because of the system symmetry. From Fig. 10, one can see the benefits of the feedforward term w.r.t. to point-stabilization (PT), which is slower in tracking the desired trajectory as emphasized in the zoom plot of the component z_L . This is because the desired velocity \mathbf{u} is updated only when a new measurement arrives. As for feedforward techniques, the two SIKM strategies yield the best performances. This can be seen in the zoom plot of z_L , where FF causes an overshoot.

More interesting and general is the comparison of the four strategies for different sampling times. To compute the feedback gain k_{off} used in the SIKM-D, we first estimated the parameters $[\mu, \alpha, \gamma_1, \gamma_2] = [0.02, 0.13, 0.1, 0.2]$ along the desired trajectory depicted in Fig. 10 for different couples of (k, T) as described in Sec. 4.1, obtaining the stability region depicted in Fig. 11. Then, for each value of T , we chose the gain k which ensures the highest convergence rate while keeping the system stable, by choosing the x coordinate corresponding to T on the curve $\tau(k_o)$ in Fig. 11. Table 2

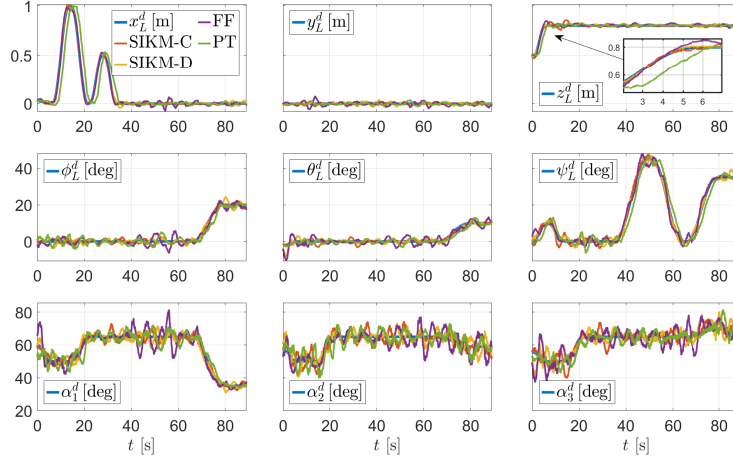


Fig. 10. Comparison of the variables $\mathbf{q}(t)$ in four different simulations, where the tracking strategies described in Table 1 are used. The sampling time is $T = 1.5[s]$. The first two rows represent respectively the position x_L, y_L, z_L and orientation ϕ_L, θ_L, ψ_L (roll, pitch and yaw) of the load. On the bottom, row the angles $\alpha_i \stackrel{\text{def}}{=} q_i$, $i = 1, 2, 3$ between cables and load are depicted.

Sampling time $T[s]$	Mean tracking error norm			
	SIKM-D	SIKM-C	FF	PT
0.5	0.06	0.05	0.05	0.07
0.75	0.06	0.07	0.06	0.10
1.5	0.10	0.09	0.15	0.16

Table 2
Mean tracking error norms obtained in simulation.

reports the observed mean tracking error norms for each strategy. The resulting feedback gain–sampling time pairs (k_{off}, T) were $(2, 0.5)$, $(1.28, 0.75)$ and $(0.67, 1.5)$. Point-stabilization PT yields the largest error which increases quickly with the sampling time. All feedback-feedforward strategies are comparable for short values of T , while SIKM-C and SIKM-D yield the lowest errors for large T . However, we stress that *SIKM-D* is *decentralized*. Hence, the results shown in Table 2 must be intended in an even stronger way: our proposed decentralized controller not only outperforms centralized implementations of standard techniques (point-stabilization and naive feedforward), but is even comparable with its centralized version with online gain computation.

To further validate our method under realistic conditions, we simulated the system with higher noise in the position measurements, comparable to a GPS-based positioning system. As expected, the tracking error remains bounded, proving our design robust. Detailed results are provided in Appendix E.

6 Conclusions and Future Work

In this paper, we proposed a decentralized controller for multi-robot systems where feedback measurements are transmitted via wireless. We showed that computing the

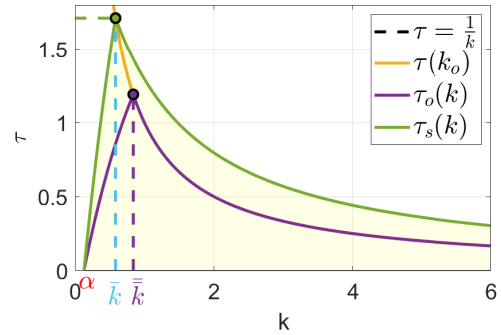


Fig. 11. Stability region, optimal gain k_o , and sampling time τ_o obtained by estimating the parameters $\mu, \alpha, \gamma_1, \gamma_2$ along the trajectory depicted in Fig. 10 for different couples (k, T) .

feedforward term is nontrivial, and proposed a strategy to compute the feedback gain with provable stability and convergence guarantees. The more multi-robot systems will become popular and employed for real application, the more sampled-based control strategies will be needed. In this sense, this work paves the way to future developments and practical implementations.

A natural evolution of this work is the implementation of experiments on a real system. Furthermore, an analysis including packets loss and latency, which are typical issues of wireless communication, should be developed.

References

- [1] G. Antonelli and S. Chiaverini. Kinematic control of platoons of autonomous vehicles. *IEEE Trans. Robot.*, 22(6):1285–1292, 2006.
- [2] T. Arai, E. Pagello, L. E. Parker, et al. Advances in multi-robot systems. *IEEE Trans. Robot. Autom.*, 18(5):655–661, 2002.

- [3] R. Conti, E. Meli, A. Ridolfi, and B. Allotta. An innovative decentralized strategy for i-auvs cooperative manipulation tasks. *Robotics and autonomous systems*, 72:261–276, 2015.
- [4] J. Cortés and M. Egerstedt. Coordinated control of multi-robot systems: A survey. *SICE Journal of Control, Measurement, and System Integration*, 10(6):495–503, 2017.
- [5] D. V. Dimarogonas and K. J. Kyriakopoulos. Distributed cooperative control and collision avoidance for multiple kinematic agents. In *45th IEEE Conf. on Decision and Control*, pages 721–726. IEEE, 2006.
- [6] S. Erhart and S. Hirche. Internal force analysis and load distribution for cooperative multi-robot manipulation. *IEEE Trans. Robot.*, 31(5):1238–1243, 2015.
- [7] H. Farivarnejad and S. Berman. Stability and convergence analysis of a decentralized proportional-integral control strategy for collective transport. In *American Control Conf.*, pages 2794–2801. IEEE, 2018.
- [8] A. Franchi and P. R. Giordano. Online leader selection for improved collective tracking and formation maintenance. *IEEE Control Netw. Syst.*, 5(1):3–13, 2018.
- [9] A. Franchi, C. Masone, V. Grabe, M. Ryll, H. H. Bühlhoff, and P. Robuffo Giordano. Modeling and control of uav bearing formations with bilateral high-level steering. *The Int. J. of Robot. Research*, 31(12):1504–1525, 2012.
- [10] A. Franchi, A. Petitti, and A. Rizzo. Distributed estimation of state and parameters in multi-agent cooperative load manipulation. *IEEE Control Netw. Syst.*, 6(2):690–701, 2019.
- [11] C. Gabellieri, M. Tognon, D. Sanalidro, L. Palottino, and A. Franchi. A study on force-based collaboration in swarms. *Swarm Intelligence*, 14:57–82, 2020.
- [12] T. Hayakawat, T. Matsuzawat, and S. Harat. Formation control of multi-agent systems with sampled information – relationship between information exchange structure and control performance –. In *45th IEEE Conf. on Decision and Control*, pages 4333–4338, 2006.
- [13] T. Lee, M. Leoky, and N. H. McClamroch. Geometric tracking control of a quadrotor UAV on SE(3). In *49th IEEE Conf. on Decision and Control*, pages 5420–5425, Atlanta, GA, Dec. 2010.
- [14] Z. Liu, W. Chen, J. Lu, H. Wang, and J. Wang. Formation control of mobile robots using distributed controller with sampled-data and communication delays. *IEEE Trans. Control Syst. Technol.*, 24(6):2125–2132, 2016.
- [15] M. Manubens, D. Devaurs, L. Ros, and J. Cortés. Motion planning for 6-D manipulation with aerial towed-cable systems. In *Robotics: Science and Systems*, Berlin, Germany, May 2013.
- [16] C. Masone, H. H. Bühlhoff, and P. Stegagno. Cooperative transportation of a payload using quadrotors: A reconfigurable cable-driven parallel robot. In *IEEE/RSJ Int. Conf. Intelligent Robots and Systems*, pages 1623–1630, Oct 2016.
- [17] I. Maza, K. Kondak, M. Bernard, and A. Ollero. Multi-UAV cooperation and control for load transportation and deployment. *J. Intell. Robot. Syst.*, 57(1-4):417–449, 2010.
- [18] D. Mellinger, M. Shomin, N. Michael, and V. Kumar. Cooperative grasping and transport using multiple quadrotors. In *Distributed autonomous robotic systems*, pages 545–558. Springer, 2013.
- [19] G. A. Pereira, M. F. Campos, and V. Kumar. Decentralized algorithms for multi-robot manipulation via caging. *Int. J. Rob. Res.*, 23(7-8):783–795, 2004.
- [20] Y. Ren, S. Sosnowski, and S. Hirche. Fully distributed cooperation for networked uncertain mobile manipulators. *IEEE Trans. Robot.*, 36(4):984–1003, 2020.
- [21] E. Rossi, M. Tognon, R. Carli, L. Schenato, J. Cortés, and A. Franchi. Cooperative aerial load transportation via sampled communication. *IEEE Contr. Syst. Lett.*, 4(2):277–282, 2020.
- [22] L. Sabattini, C. Secchi, N. Chopra, and A. Gasparri. Distributed control of multirobot systems with global connectivity maintenance. *IEEE Trans. on Robotics*, 29(5):1326–1332, 2013.
- [23] D. Sanalidro, H. J. Savino, M. Tognon, J. Cortés, and A. Franchi. Full-pose manipulation control of a cable-suspended load with multiple uavs under uncertainties. *IEEE Robot. Autom. Lett.*, 5:2185–2191, January 2020.
- [24] M. Schwager, B. J. Julian, M. Angermann, and D. Rus. Eyes in the sky: Decentralized control for the deployment of robotic camera networks. *Proc. IEEE*, 99(9):1541–1561, 2011.
- [25] B. Siciliano, L. Sciavicco, L. Villani, and G. Oriolo. *Robotics: Modelling, Planning and Control*. Springer, 2009.
- [26] D. Sieber and S. Hirche. Human-guided multirobot cooperative manipulation. *IEEE Trans. Control Syst. Technol.*, 27(4):1492–1509, 2019.
- [27] E. Simetti and G. Casalino. Manipulation and transportation with cooperative underwater vehicle manipulator systems. *IEEE J. Ocean. Eng.*, 42(4):782–799, 2016.
- [28] K. Sreenath and V. Kumar. Dynamics, control and planning for cooperative manipulation of payloads suspended by cables from multiple quadrotor robots. In *Robotics: Science and Systems*, Berlin, Germany, June 2013.
- [29] S. Stramigioli, C. Secchi, A. J. van der Schaft, and C. Fantuzzi. Sampled data systems passivity and discrete port-hamiltonian systems. *IEEE Trans. Robot.*, 21(4):574–587, 2005.
- [30] A. Tagliabue, M. Kamel, R. Siegwart, and J. Nieto. Robust collaborative object transportation using multiple mavs. *Int. J. Rob. Res.*, 38(9):1020–1044, 2019.
- [31] M. Tognon, C. Gabellieri, L. Pallottino, and A. Franchi. Aerial co-manipulation with cables: The role of internal force for equilibria, stability, and passivity. *IEEE Robotics and Automation Letters, Special Issue on Aerial Manipulation*, 3(3):2577 – 2583, 2018.
- [32] A. Tsiamis, C. K. Verginis, C. P. Bechlioulis, and K. J. Kyriakopoulos. Cooperative manipulation exploiting only implicit communication. In *IEEE/RSJ Int. Conf. Intell. Robots Syst.*, pages 864–869. IEEE, 2015.
- [33] C. K. Verginis, A. Nikou, and D. V. Dimarogonas. Communication-based decentralized cooperative object transportation using nonlinear model predictive control. In *European Control Conf.*, pages 733–738. IEEE, 2018.
- [34] Z. Wang and M. Schwager. Force-amplifying n-robot transport system (force-ants) for cooperative planar manipulation without communication. *Int. J. Rob. Res.*, 35(13):1564–1586, 2016.

A Useful Lemmas

Lemma A.1 *Given $\mathbf{x} \in \mathcal{X}$, where $\mathcal{X} \subset \mathbb{R}^n$ is a compact set and given a continuously differentiable function $\mathbf{f}(\mathbf{x}) : \mathbb{R}^n \rightarrow \mathbb{R}^m$ s.t. $\mathbf{f}(\mathbf{0}) = \mathbf{0}$, then there exists $\alpha > 0$ s.t.:*

$$\|\mathbf{f}(\mathbf{x})\| \leq \alpha \|\mathbf{x}\| \quad \forall \mathbf{x} \in \mathcal{X}.$$

PROOF. Since $\mathbf{f}(\mathbf{x})$ is a continuously differentiable function on a compact set, then it is Lipschitz continuous and it holds

$$\mathbf{f}(\mathbf{x}_1 - \mathbf{x}_2) \leq \alpha \|\mathbf{x}_1 - \mathbf{x}_2\|,$$

for some $\alpha > 0$. Now let us call $\mathbf{x} := \mathbf{x}_1$ and $\mathbf{x}_2 = \mathbf{0}$ and we obtain the result of the Lemma.

Lemma A.2 *Given $\mathbf{x} \in \mathcal{X}$ and $\mathbf{y} \in \mathcal{Y}$, where $\mathcal{X} \subset \mathbb{R}^n$, $\mathcal{Y} \subset \mathbb{R}^p$ are compact sets and given a function that is continuously differentiable on the second argument $\mathbf{f}(\mathbf{x}, \mathbf{y}) : \mathbb{R}^n \times \mathbb{R}^p \rightarrow \mathbb{R}^m$ s.t. $\mathbf{f}(\mathbf{x}, \mathbf{0}) = \mathbf{0} \forall \mathbf{x} \in \mathcal{X}$, then there exists $\alpha > 0$ s.t.:*

$$\|\mathbf{f}(\mathbf{x}, \mathbf{y})\| \leq \alpha \|\mathbf{y}\| \quad \forall (\mathbf{x}, \mathbf{y}) \in \mathcal{X} \times \mathcal{Y}.$$

PROOF. The proof is similar to the one of Lemma A.1: being the function continuously differentiable in the second argument, we apply that reasoning on \mathbf{y} :

$$\|\mathbf{f}(\mathbf{x}, \mathbf{y}_1 - \mathbf{y}_2)\| \leq \alpha \|\mathbf{y}_1 - \mathbf{y}_2\|,$$

for some $\alpha > 0$. Now let us call $\mathbf{y} := \mathbf{y}_1$ and $\mathbf{y}_2 = \mathbf{0}$ and we obtain the result of the Lemma.

Lemma A.3 *Given $\mathbf{x} \in \mathcal{X}$, where $\mathcal{X} \subset \mathbb{R}^n$ is a compact set and given two continuously differentiable functions $\mathbf{f}(\mathbf{x}) : \mathbb{R}^n \rightarrow \mathbb{R}^m$, $\mathbf{g}(\mathbf{x}) : \mathbb{R}^n \rightarrow \mathbb{R}^m$ s.t. $\mathbf{f}(\mathbf{0}) = \mathbf{g}(\mathbf{0}) = \mathbf{0}$, then there exists $\alpha > 0$ s.t.:*

$$\|\mathbf{f}(\mathbf{x}) \cdot \mathbf{g}(\mathbf{x})\| \leq \alpha \|\mathbf{x}\|^2 \quad \forall \mathbf{x} \in \mathcal{X}.$$

PROOF. The proof is similar to the one of Lemma A.1. Since both the functions are continuously differentiable on a compact set, then they are also Lipschitz and there exist $a, b > 0$ s.t.

$$\|\mathbf{f}(\mathbf{x})\| \leq a \|\mathbf{x}\|, \quad \|\mathbf{g}(\mathbf{x})\| \leq b \|\mathbf{x}\|,$$

hence

$$\|\mathbf{f}(\mathbf{x}) \cdot \mathbf{g}(\mathbf{x})\| \leq \|\mathbf{f}(\mathbf{x})\| \cdot \|\mathbf{g}(\mathbf{x})\| \leq \alpha \|\mathbf{x}\|^2,$$

where $\alpha := ab > 0$ and we obtain the result of the lemma.

B Error Bound for Point-Stabilization Control

In [21], the authors discussed how, given a desired constant configuration \mathbf{q}^r , if $\mathbf{q}(0) \in \mathcal{B}_d(\mathbf{q}^r)$, the gain k can be designed offline s.t. \mathbf{u}_k in (10) drives the system state to \mathbf{q}^r exponentially fast.

To perform trajectory tracking, the same idea is replicated by assigning a sequence of points as a time-varying

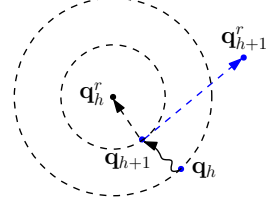


Fig. B.1. Trajectory tracking by using the point stabilization strategy.

reference to the system. In particular, the reference trajectory $\mathbf{q}^r(t)$ is sampled with period T , and the sample points of the sequence $(\mathbf{q}^r(hT), \dot{\mathbf{q}}^r(hT))$ are given as reference configurations one after the other. Such a strategy is indeed commonly used in robotic applications in virtue of its simplicity. The control law becomes (cf. (10))

$$\mathbf{u}(t) = \mathbf{u}_k(hT) = -k\mathbf{A}_{\mathbf{q}(hT)}(\mathbf{q}(hT) - \mathbf{q}^r(hT)),$$

with $t \in [hT, (h+1)T)$. When k is assigned offline, the tracking error is characterized as follows.

Proposition 16 *Consider system (2)–(4) with $\mathbf{u}(t)$ given by (11). There exist $0 < \rho < 1$ and k^* such that, if $\mathbf{q}(0) \in \mathcal{B}_d(\mathbf{q}^r(0))$, $\|\mathbf{q}^r((h+1)T) - \mathbf{q}^r(hT)\| \leq \beta$ for all h with $0 < \beta < (1-\rho)d$, and $0 < k < k^*$, then the tracking error $\mathbf{e}(hT) \stackrel{\text{def}}{=} \mathbf{q}(hT) - \mathbf{q}^r(hT)$ is bounded, i.e.,*

$$\|\mathbf{e}(hT)\| \leq \rho d + \frac{\beta}{1-\rho}, \quad \forall h \in \mathbb{N},$$

and in particular

$$\lim_{h \rightarrow +\infty} \|\mathbf{e}(hT)\| \leq \frac{\beta}{1-\rho}.$$

PROOF. As shown in Fig. B.1, at time $t = hT$ the system state is $\mathbf{q}_h = \mathbf{q}(hT)$ and the reference point is \mathbf{q}^r_h ; then, at time $t = (h+1)T$, the new system state is $\mathbf{q}_{h+1} = \mathbf{q}((h+1)T)$ and a new reference \mathbf{q}^r_{h+1} is assigned. This strategy is applied every T seconds. In [21, Proposition 6] the authors showed that, given a configuration \mathbf{q}_h and the desired one \mathbf{q}^r_h , there exists a feedback gain s. t.

$$\|\mathbf{e}((h+1)T)\| \leq \rho_h \|\mathbf{e}(hT)\|, \quad (\text{B.1})$$

where $\rho_h \in (0, 1)$ is defined in [21, Proposition 5] and depends on the set $\mathcal{B}_d(\mathbf{q}^r(hT))$. In virtue of Assumption 1.i), we consider $\rho = \max_h \rho_h$ as an upper bound for the convergence rate over all the trajectory samples. Equation (B.1) implies that the error decreases by at least a factor ρ between two consecutive sampling times. Further, it is shown in [21] that the error also decreases at each time instant $t \in (hT, (h+1)T)$. Now, we define

the quantities

$$\mathbf{e}_{h+1}^+ \stackrel{\text{def}}{=} \mathbf{q}_{h+1} - \mathbf{q}_{h+1}^r, \quad \mathbf{e}_{h+1}^- \stackrel{\text{def}}{=} \mathbf{q}_{h+1} - \mathbf{q}_h^r.$$

In words, \mathbf{e}_{h+1}^- is the error between configuration \mathbf{q}_{h+1} and the desired one \mathbf{q}_h^r , while \mathbf{e}_{h+1}^+ is the error between \mathbf{q}_{h+1} and the next desired configuration \mathbf{q}_{h+1}^r . In view of (B.1) and assumption $\|\mathbf{q}_{h+1}^r - \mathbf{q}_h^r\| \leq \beta$, it holds

$$\begin{aligned} \|\mathbf{e}_{h+1}^-\| &= \|\mathbf{q}_{h+1} - \mathbf{q}_h^r\| \leq \rho \|\mathbf{q}_h - \mathbf{q}_h^r\| = \rho \|\mathbf{e}_h^+\| \\ \|\mathbf{e}_{h+1}^+\| &= \|\mathbf{q}_{h+1} - \mathbf{q}_h^r + \mathbf{q}_h^r - \mathbf{q}_{h+1}^r\| \\ &\leq \|\mathbf{q}_{h+1} - \mathbf{q}_h^r\| + \|\mathbf{q}_h^r - \mathbf{q}_{h+1}^r\| \\ &= \|\mathbf{e}_{h+1}^-\| + \|\mathbf{q}_h^r - \mathbf{q}_{h+1}^r\| \leq \rho \|\mathbf{e}_h^+\| + \beta. \end{aligned}$$

Being $\beta < (1 - \rho)d$, it follows $\|\mathbf{e}_{h+1}^+\| < d$ and therefore Proposition 6 in [21] can be applied s.t. the error decrease (B.1) holds for reference point \mathbf{q}_{h+1}^r in an iterative fashion. Now, we find an upper bound to the steady-state tracking error: iterating the last inequality, it holds

$$\begin{aligned} \|\mathbf{e}_1^+\| &\leq \rho \|\mathbf{e}_0^+\| + \beta \\ \|\mathbf{e}_2^+\| &\leq \rho \|\mathbf{e}_1^+\| + \beta \leq \rho^2 \|\mathbf{e}_0^+\| + \rho\beta + \beta \\ &\vdots \\ \|\mathbf{e}_h^+\| &\leq \rho^h \|\mathbf{e}_0^+\| + \beta \sum_{i=0}^{h-1} \rho^i = \rho^h \|\mathbf{e}_0^+\| + \beta \frac{1 - \rho^h}{1 - \rho}. \end{aligned}$$

The overall upper bound for the error norm can be deduced in virtue of the assumptions $\|\mathbf{e}_0^+\| < d$ and $\rho < 1$. In particular, at the limit it follows

$$\lim_{h \rightarrow +\infty} \|\mathbf{e}_h^+\| \leq \lim_{h \rightarrow +\infty} \beta \frac{1 - \rho^h}{1 - \rho} = \frac{\beta}{1 - \rho}. \quad \square$$

C Proofs of Propositions 9–11

C.1 Proof of Proposition 9

Recall that the stability time $\tau_s(k)$ is s.t. $z(k, \tau) < 1$ for $k > \alpha, 0 < \tau < \tau_s(k)$. Hence the goal now is to find an expression for $\tau_s(k)$ by studying the inequality

$$z(k, \tau) < 1,$$

From the definition of the function $z(k, \tau)$, we can distinguish three cases: $k\tau < 1$, $k\tau = 1$, $k\tau > 1$.

(1) $k\tau < 1$: In this case

$$z(k, \tau) = z^-(k, \tau) = 1 + \tau(\alpha - k) + \tau^2(k^2\mu + k\gamma_1 + \gamma_2).$$

We are interested to understand when $z^-(k, \tau) < 1$, that is to find the maximum τ for which $\|\mathbf{e}(hT + \tau)\| < \|\mathbf{e}(hT)\|$.

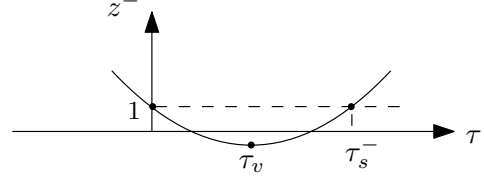


Fig. C.1. Representation of $z(k, \tau)$ in the case $k\tau < 1$ and $k > \alpha$.

$$z^-(k, \tau) < 1$$

$$\Leftrightarrow 1 + \tau(\alpha - k) + \tau^2(k^2\mu + k\gamma_1 + \gamma_2) < 1$$

$$\Leftrightarrow p_s^-(k) := \tau(\alpha - k) + \tau^2(k^2\mu + k\gamma_1 + \gamma_2) < 0.$$

$p_s^-(k)$ represents an upward parabola with solutions

$$\tau_{s1}^- = 0, \quad \tau_{s2}^- = \frac{k - \alpha}{k^2\mu + k\gamma_1 + \gamma_2}.$$

Hence $p_s^-(k) < 0$ if $0 < \tau < \tau_{s2}^-$; as a consequence $z^-(k, \tau) < 1$ if $0 < \tau < \tau_{s2}^-$. Let us define

$$\tau_s^- := \tau_{s2}^-.$$

Now let us check when $\tau_s^- < \frac{1}{k}$, that is

$$\frac{k - \alpha}{k^2\mu + k\gamma_1 + \gamma_2} < \frac{1}{k}$$

$$\Leftrightarrow p_{s2}^-(k) := k^2(1 - \mu) - k(\alpha + \gamma_1) - \gamma_2 < 0.$$

The solutions are

$$k_{s1,2}^- = \frac{\alpha + \gamma_1 \pm \sqrt{(\alpha + \gamma_1)^2 + 4\gamma_2(1 - \mu)}}{2(1 - \mu)}.$$

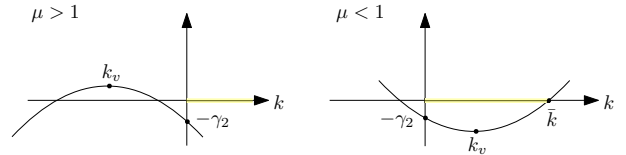


Fig. C.2. Representation of $p_{s2}^-(k)$.

- if $\mu < 1$, then $p_{s2}^-(k)$ is an upward parabola such that the solutions and the vertex k_v satisfy

$$\sum \text{sol} = \frac{\alpha + \gamma_1}{1 - \mu} > 0, \quad \prod \text{sol} = \frac{-\gamma_2}{1 - \mu} < 0$$

$$k_v = \frac{\alpha + \gamma_1}{2(1 - \mu)} > 0.$$

Hence, if $\mu < 1$, then $\tau_s^- < \frac{1}{k}$ for $\alpha < k < \bar{k}$, where

$$\bar{k} = \max\{k_{s_1}^-, k_{s_2}^-\} = \begin{cases} \frac{\alpha + \gamma_1 + \sqrt{(\alpha + \gamma_1)^2 + 4\gamma_2(1-\mu)}}{2(1-\mu)} & \text{if } \mu < 1 \\ \frac{\alpha + \gamma_1 - \sqrt{(\alpha + \gamma_1)^2 + 4\gamma_2(1-\mu)}}{2(1-\mu)} & \text{if } \mu > 1 \end{cases} \quad (\text{C.1})$$

In this case $\mu < 1$, hence $\bar{k} = \frac{\alpha + \gamma_1 + \sqrt{(\alpha + \gamma_1)^2 + 4\gamma_2(1-\mu)}}{2(1-\mu)}$.

- if $\mu > 1$, then $p_{s_2}^-(k)$ is a downward parabola such that

$$\sum \text{sol} < 0, \quad \prod \text{sol} > 0$$

$$k_v < 0.$$

Hence, if $\mu > 1$, then $\tau_s^- < \frac{1}{k} \quad \forall \quad k > \alpha$. In conclusion,

$$z^-(k, \tau) < 1 \text{ if } 0 < \tau < \tau_s^-$$

$$\tau_s^- < \frac{1}{k} \text{ if } \begin{cases} \alpha < k < \bar{k} & \text{if } \mu < 1 \\ k > \alpha & \text{if } \mu > 1 \end{cases}$$

(2) $k\tau = 1$: In this case

$$z\left(k, \frac{1}{k}\right) = \mu + \frac{1}{k}(\alpha + \gamma_1) + \frac{\gamma_2}{k^2}.$$

For which values of k is $z(k, \frac{1}{k}) < 1$?

$$\mu + \frac{1}{k}(\alpha + \gamma_1) + \frac{\gamma_2}{k^2} < 1$$

$$p_s^-(k) := k^2(\mu - 1) + k(\alpha + \gamma_1) + \gamma_2 < 0. \quad (\text{C.2})$$

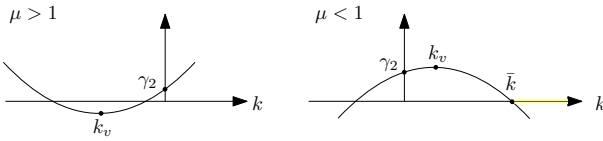


Fig. C.3. Representation of p_s^- .

- $\mu < 1$: p_s^- is a concave downward parabola. In $k = 0$ the parabola intersects the y-axis in $\gamma_2 > 0$. Now the vertex of the parabola is in $k_v^- > 0$, the sum of the solutions is $\sum \text{sol} > 0$ and product $\prod \text{sol} < 0$. Finally, $z(k, \frac{1}{k}) < 1$ where $p_s^-(k) < 0$, that is for $k > \bar{k}$, where $\bar{k} := \max\{k_{s_1}^-, k_{s_2}^-\}$ has the same value that we have found in (C.1).
- $\mu > 1$: p_s^- is a concave upward parabola. In $k = 0$ the parabola intersects the y-axis in $\gamma_2 > 0$. The vertex of the parabola is in

$$k_v^- = \frac{\alpha + \gamma_1}{2(1-\mu)} < 0.$$

The sum and product of the solutions are

$$\sum \text{sol} = \frac{\alpha + \gamma_1}{1 - \mu} < 0, \quad \prod \text{sol} = \frac{\gamma_2}{\mu - 1} > 0,$$

hence the solutions are both negative and $p_s^-(k)$ is always positive, so $z(k, \frac{1}{k}) > 1 \quad \forall k > \alpha$ if $\mu > 1$.

In conclusion:

$$z(k, 1/k) < 1 \text{ for } \begin{cases} \nexists k > \alpha & \text{if } \mu > 1 \\ k > \bar{k} & \text{if } \mu < 1 \end{cases}.$$

(3) $k\tau > 1$: In this case

$$z(k, \tau) = z^+(k, \tau) = -1 + \tau(\alpha + k) + \tau^2(k^2\gamma_1 + k\gamma_2 + \gamma_3).$$

This is an upward parabola with vertex

$$\tau_v^+ = -\frac{k + \alpha}{2(k^2\gamma_1 + k\gamma_2 + \gamma_3)} < 0$$

Notice that $z^+(k, 0) = -1 < 0$ and

$$\sum \text{sol} = -\frac{\alpha + k}{k^2\mu + k\gamma_1 + \gamma_2} < 0$$

$$\prod \text{sol} = -\frac{1}{k^2\mu + k\gamma_1 + \gamma_2} < 0.$$

For which values of k is $z^+(k, \tau) < 1$?

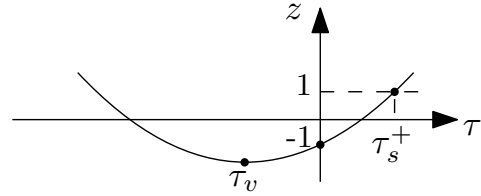


Fig. C.4. Representation of $z(k, \tau)$ in the case $k\tau > 1$.

$$z^+(k, \tau) < 1$$

$$\Leftrightarrow -1 + \tau(\alpha + k) + \tau^2(k^2\mu + k\gamma_1 + \gamma_2) < 1$$

$$\Leftrightarrow p_s^+(k) := \tau^2(k^2\mu + k\gamma_1 + \gamma_2) + \tau(\alpha + k) - 2 < 0.$$

$p_s^+(k)$ represents an upward parabola with solutions s.t.

$$\sum \text{sol} = -\frac{\alpha + k}{k^2\mu + k\gamma_1 + \gamma_2} < 0$$

$$\prod \text{sol} = -\frac{2}{k^2\mu + k\gamma_1 + \gamma_2} < 0$$

$$\tau_{s_1}^+ = \frac{-(\alpha + k) - \sqrt{(\alpha + k)^2 + 8(k^2\mu + k\gamma_1 + \gamma_2)}}{2(k^2\mu + k\gamma_1 + \gamma_2)}$$

$$\tau_{s_2}^+ = \frac{-(\alpha + k) + \sqrt{(\alpha + k)^2 + 8(k^2\mu + k\gamma_1 + \gamma_2)}}{2(k^2\mu + k\gamma_1 + \gamma_2)}$$

We define

$$\tau_s^+ := \max\{\tau_{s_1,2}^+\} = \tau_{s_2}^+$$

and $z^+(k, \tau) < 1$ for $0 < \tau < \tau_s^+$. Notice that in this case we have to check for which k it holds $\tau_s^+ > \frac{1}{k}$ since we are analyzing the case $k\tau > 1$:

$$\begin{aligned} \tau_s^+ &> \frac{1}{k} \\ \frac{-(\alpha + k) + \sqrt{(\alpha + k)^2 + 8(k^2\mu + k\gamma_1 + \gamma_2)}}{2(k^2\mu + k\gamma_1 + \gamma_2)} &> \frac{1}{k} \\ -k(\alpha + k) + k\sqrt{(\alpha + k)^2 + 8(k^2\mu + k\gamma_1 + \gamma_2)} &> 2(k^2\mu + k\gamma_1 + \gamma_2) \\ &> 2(k^2\mu + k\gamma_1 + \gamma_2) \\ k^2((\alpha + k)^2 + 8(k^2\mu + k\gamma_1 + \gamma_2)) &> k^2(\alpha + k)^2 + \\ &+ 4(k^2\mu + k\gamma_1 + \gamma_2)^2 + 4k(\alpha + k)(k^2\mu + k\gamma_1 + \gamma_2) \\ 8k^2(k^2\mu + k\gamma_1 + \gamma_2) &> 4(k^2\mu + k\gamma_1 + \gamma_2)^2 + \\ &+ 4k(\alpha + k)(k^2\mu + k\gamma_1 + \gamma_2) \\ 2k^2 &> (k^2\mu + k\gamma_1 + \gamma_2) + k(\alpha + k) \\ k^2(1 - \mu) - k(\alpha + \gamma_1) - \gamma_2 &> 0 \\ p_{\tau_s^+}(k) &:= k^2(\mu - 1) + k(\alpha + \gamma_1) + \gamma_2 < 0 \end{aligned}$$

The solutions are

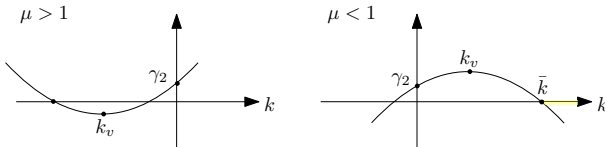


Fig. C.5. Representation of $p_{\tau_s^+}(k)$.

$$k_{\pm} = \frac{\alpha + \gamma_1 \pm \sqrt{(\alpha + \gamma_1)^2 + 4\gamma_2(1 - \mu)}}{2(1 - \mu)}$$

- $\mu > 1$: $p_{\tau_s^+}(k)$ is an upward parabola s.t. for $k = 0$ it intersects the y-axis in γ_2 and

$$\sum \text{sol} = -\frac{\alpha + \gamma_1}{\mu - 1} < 0, \quad \prod \text{sol} = \frac{\gamma_2}{\mu - 1} < 0$$

As a consequence, this parabola is never negative for $k > 0$, hence $\tau_s^+ < \frac{1}{k} \forall k > 0$.

- $\mu < 1$: $p_{\tau_s^+}(k)$ is a downward parabola and

$$\sum \text{sol} > 0, \quad \prod \text{sol} > 0$$

As a consequence, it is negative for $k > \bar{k}$, hence $\tau_s^+ > \frac{1}{k}$ for $k > \bar{k} = \max\{k_{\pm}\}$, that is the same value found in (C.1).

In conclusion,

$$z^+(k, \tau) < 1 \text{ if } 0 < \tau < \tau_s^+$$

$$\tau_s^+ \begin{cases} < \frac{1}{k} & \text{for } k > \alpha \quad \text{if } \mu > 1 \\ > \frac{1}{k} & \text{for } k > \bar{k} \quad \text{if } \mu < 1 \end{cases}$$

Notice that only if $\mu < 1$, then τ_s^+ belongs to the region $k\tau > 1$ that we are considering. Otherwise, we have to consider τ_s^- instead.

Hence $\tau_s = \tau_s^-$ if $\mu > 1$ or if $\mu < 1$ and $\alpha < k < \bar{k}$, whereas $\tau_s = \tau_s^+$ if $\mu < 1$ and $k > \bar{k}$, that is

$$\begin{aligned} \tau_s(k; \mu, \gamma_1, \gamma_2) &= \frac{k - \alpha}{k^2\mu + k\gamma_1 + \gamma_2} \text{ if } \mu > 1 \\ \tau_s(k; \mu, \gamma_1, \gamma_2) &= \begin{cases} \frac{k - \alpha}{k^2\mu + k\gamma_1 + \gamma_2} & \text{for } \alpha < k < \bar{k} \\ \frac{-(\alpha + k) + \sqrt{(\alpha + k)^2 + 8(k^2\mu + k\gamma_1 + \gamma_2)}}{2(k^2\mu + k\gamma_1 + \gamma_2)} & \text{for } k > \bar{k} \end{cases} \text{ if } \mu < 1 \end{aligned}$$

C.2 Proof of Proposition 10

Recall that the optimal time $\tau_o(k)$ is s.t. $z(k, \tau_o(k))$ reaches its minimum value. Hence the goal now is to find an expression for $\tau_o(k)$.

From the definition of the function $z(k, \tau)$, we can distinguish two cases: $k\tau < 1$, $k\tau > 1$.

- (1) $k\tau < 1$: In this case

$$z(k, \tau) = z^-(k, \tau) = 1 + \tau(\alpha - k) + \tau^2(k^2\mu + k\gamma_1 + \gamma_2)$$

$z(k, \tau)$ is an upward parabola (see Fig. C.1) with vertex at

$$\tau_v^- = \frac{k - \alpha}{2(k^2\mu + k\gamma_1 + \gamma_2)} \quad (\text{C.3})$$

Notice that $\tau_v^- > 0$ since $k > \alpha$. The value of the function at the vertex corresponds to its minimum:

$$\begin{aligned} z(k, \tau_v) &= 1 - \frac{(k - \alpha)^2}{2(k^2\mu + k\gamma_1 + \gamma_2)} + \\ &+ \frac{(k - \alpha)^2}{4(k^2\mu + k\gamma_1 + \gamma_2)^2} (k^2\mu + k\gamma_1 + \gamma_2) = \\ &= 1 - \frac{1}{4} \frac{(k - \alpha)^2}{(k^2\mu + k\gamma_1 + \gamma_2)} < 1 \end{aligned}$$

Now we want to check if $\tau_v^- < \frac{1}{\bar{k}}$, that is if the minimum value belongs to the region we are analyzing:

$$\begin{aligned}\tau_v^- &= \frac{k - \alpha}{2(k^2\mu + k\gamma_1 + \gamma_2)} < \frac{1}{\bar{k}} \\ \Leftrightarrow k^2 - k\alpha &< 2\mu k^2 + 2\gamma_1 k + 2\gamma_2 \\ \Leftrightarrow p_v^-(k) &:= k^2(1 - 2\mu) - k(\alpha + 2\gamma_1) - 2\gamma_2 < 0\end{aligned}\quad (\text{C.4})$$

where the solutions of $p_v^-(k)$

$$k_{\pm} = \frac{\alpha + 2\gamma_1 \pm \sqrt{(\alpha + 2\gamma_1)^2 + 8\gamma_2(1 - 2\mu)}}{2(1 - 2\mu)}$$

are s.t.

$$\sum \text{sol} = \frac{\alpha + 2\gamma_1}{1 - 2\mu}, \quad \prod \text{sol} = \frac{-2\gamma_2}{1 - 2\mu}$$

where there exist two different solutions if $(\alpha + 2\gamma_1)^2 + 8\gamma_2(1 - 2\mu) > 0$, that is

$$\mu < \frac{(\alpha + 2\gamma_1)^2}{16\gamma_2} + \frac{1}{2}$$

otherwise τ_v^- is always greater than $1/k$.

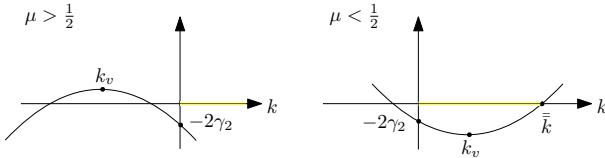


Fig. C.6. Representation of $p_v^-(k)$.

- if $1 - 2\mu > 0$, that is $\mu < \frac{1}{2}$, then $p_v^-(k)$ is an upward parabola with solutions k_{\pm} s.t. $\sum \text{sol} > 0$, $\prod \text{sol} < 0$ and $\tau_v < \frac{1}{\bar{k}}$ if $\alpha < k < \bar{k}$, where

$$\begin{aligned}\bar{k} &:= \max\{k_-, k_+\} = \\ &= \begin{cases} \frac{\alpha + 2\gamma_1 + \sqrt{(\alpha + 2\gamma_1)^2 + 8\gamma_2(1 - 2\mu)}}{2(1 - 2\mu)} & \text{if } \mu < \frac{1}{2} \\ \frac{\alpha + 2\gamma_1 - \sqrt{(\alpha + 2\gamma_1)^2 + 8\gamma_2(1 - 2\mu)}}{2(1 - 2\mu)} & \text{if } \mu > \frac{1}{2} \end{cases}\end{aligned}\quad (\text{C.5})$$

- if $1 - 2\mu < 0$, that is $\mu > \frac{1}{2}$, then $p_v^-(k)$ is a downward parabola with solutions k_{\pm} s.t. $\sum \text{sol} < 0$, $\prod \text{sol} > 0$ and $\tau_v < \frac{1}{\bar{k}}$ if $k > \alpha$.

In conclusion,

$$\tau_v^- < \frac{1}{\bar{k}} \text{ if } \begin{cases} \alpha < k < \bar{k} & \text{if } \mu < \frac{1}{2} \\ k > \alpha & \text{if } \mu > \frac{1}{2} \end{cases}$$

So τ_v^- represents the optimal time in the case $k\tau < 1$ for $\alpha < k < \bar{k}$ if $\mu < \frac{1}{2}$ and for $k > \alpha$ if $\mu > \frac{1}{2}$.

(2) $k\tau > 1$. In this case

$$z(k, \tau) = z^+(k, \tau) = -1 + \tau(\alpha + k) + \tau^2(k^2\gamma_1 + k\gamma_2 + \gamma_3)$$

we still have an upward parabola with vertex

$$\tau_v^+ = -\frac{k + \alpha}{2(k^2\gamma_1 + k\gamma_2 + \gamma_3)} < 0$$

Since $\tau_v^+ < 0$ it cannot be a valid optimal time and, since $z(k, \tau)$ is a monotonically increasing function in k and τ , then the minimum can be detected in $\tau = 1/k$.

Finally $\tau_o(k) = \tau_v^-(k)$ for $\alpha < k < \bar{k}$ if $\mu < \frac{1}{2}$ and for $k > \alpha$ if $\mu > \frac{1}{2}$, whereas $\tau_o(k) = 1/k$ for $k > \bar{k}$ if $\mu < \frac{1}{2}$, that is

$$\begin{aligned}\tau_o(k; \mu, \gamma_1, \gamma_2) &= \frac{k - \alpha}{2(k^2\mu + k\gamma_1 + \gamma_2)} \text{ if } \mu > \frac{1}{2} \\ \tau_o(k; \mu, \gamma_1, \gamma_2) &= \begin{cases} \frac{k - \alpha}{2(k^2\mu + k\gamma_1 + \gamma_2)} & \text{for } \alpha < k < \bar{k} \\ \frac{1}{k} & \text{for } k > \bar{k} \end{cases} \text{ if } \mu < \frac{1}{2}\end{aligned}$$

Computation of the convergence rate

The convergence rate, defined in (27), corresponds to the function $z(k, \tau)$ evaluated in $\tau = \tau_o(k)$:

$$\rho(k) = z(k, \tau_o)$$

We have already seen that, depending on the value of the parameter μ , then $\tau_o(k)$ has different values and $z(k, \tau_o(k))$ too:

- $0 < \mu < \frac{1}{2}$:

$$\tau_o = \begin{cases} \tau_v^- & \text{if } \alpha < k < \bar{k} \\ \frac{1}{k} & \text{if } k > \bar{k} \end{cases}$$

and

$$\begin{aligned}\rho(k) &= z^-(k, \tau_o) = \\ &= \begin{cases} z^-(k, \tau_v^-) = 1 - \frac{(\alpha - k)^2}{4(k^2\mu + k\gamma_1 + \gamma_2)} & \text{if } \alpha < k < \bar{k} \\ z(k, \frac{1}{k}) = \mu + \frac{1}{k}(\alpha + \gamma_1) + \frac{1}{k^2}\gamma_2 & \text{if } k > \bar{k} \end{cases}\end{aligned}$$

Notice that $z^-(k, \tau_o) < 1$ always and $z(k, \frac{1}{k}) < 1$ in the case it is considered ($\mu < \frac{1}{2}$). Moreover, note that for $\gamma_1 = \gamma_2 = 0$, $z^-(k, \frac{1}{k}) = \mu + \frac{\alpha}{k}$ that tends to μ for large values of k :

$$\rho(k) \rightarrow \begin{cases} 1 - \frac{1}{4\mu} & \text{if } \alpha < k < \bar{k} \\ \mu & \text{if } k > \bar{k} \end{cases}$$

- $\mu > \frac{1}{2}$: in this case

$$\rho = z^-(k, \tau_v^-) = 1 - \frac{(\alpha - k)^2}{4(k^2\mu + k\gamma_1 + \gamma_2)} \quad \forall \quad k > \alpha$$

and for $\gamma_1 = \gamma_2 = 0$ and big values of k :

$$\rho(k) \rightarrow 1 - \frac{1}{4\mu} \quad \forall \quad k > \alpha$$

C.3 Proof of Proposition 11

- (1) $k\tau < 1$:

Let us rewrite the function $z^-(k, \tau)$ s.t. it depends on k , since τ is assumed to be fixed now.

$$z^-(k, \tau) = \tau^2\mu k^2 + \tau(\tau\gamma_1 - 1)k + 1 + \tau\alpha + \tau^2\gamma_2 \quad (\text{C.6})$$

The function represents an upward parabola with vertex

$$k_v^- = \frac{1 - \tau\gamma_1}{2\tau\mu} > 0 \text{ if } \tau < \frac{1}{\gamma_1}$$

Let us check when $k_v^- < \frac{1}{\tau}$:

$$\frac{1 - \tau\gamma_1}{2\tau\mu} < \frac{1}{\tau} \quad \Leftrightarrow \quad \tau > \frac{1 - 2\mu}{\gamma_1}$$

Observe that if $\mu > \frac{1}{2}$, then $\frac{1 - 2\mu}{\gamma_1} < 0$, hence $\tau > \frac{1 - 2\mu}{\gamma_1}$ always and $k_v^- < \frac{1}{\tau}$.

In conclusion,

$$k_v^- < \frac{1}{\tau} \text{ if } \tau > \frac{1 - 2\mu}{\gamma_1}$$

Now we find out when $z^-(k_v^-, \tau) < 1$. First of all we compute the expression $z^-(k_v^-, \tau)$:

$$\begin{aligned} z^-(k_v^-, \tau) &= \tau^2\mu \frac{(1 - \tau\gamma_1)^2}{4\tau^2\mu^2} + \tau(\tau\gamma_1 - 1) \frac{1 - \tau\gamma_1}{2\tau\mu} + \tau^2\gamma_2 + \\ &\quad + \tau\alpha + 1 = \\ &= \frac{(1 - \tau\gamma_1)^2}{4\mu} - \frac{(1 - \tau\gamma_1)^2}{2\mu} + \tau^2\gamma_2 + \tau\alpha + 1 \\ &= -\frac{(1 - \tau\gamma_1)^2}{4\mu} + \tau^2\gamma_2 + \tau\alpha + 1 \\ &= \frac{(-\gamma_1^2 + 4\gamma_2\mu)\tau^2 + 2(\gamma_1 + 2\alpha\mu)\tau + 4\mu - 1}{4\mu} \end{aligned}$$

Now, under which conditions does it hold $z^-(k_v^-, \tau) < 1$?

$$\begin{aligned} \frac{(-\gamma_1^2 + 4\gamma_2\mu)\tau^2 + 2(\gamma_1 + 2\alpha\mu)\tau + 4\mu - 1}{4\mu} &< 1 \\ \Leftrightarrow (-\gamma_1^2 + 4\gamma_2\mu)\tau^2 + 2(\gamma_1 + 2\alpha\mu)\tau + 4\mu - 1 &< 4\mu \\ p_v^-(\tau) := (-\gamma_1^2 + 4\gamma_2\mu)\tau^2 + 2(\gamma_1 + 2\alpha\mu)\tau - 1 &< 0 \end{aligned} \quad (\text{C.7})$$

$p_v^-(\tau)$ is a parabola in τ with vertex in

$$\tau_v^- = -\frac{\gamma_1 + 2\alpha\mu}{-\gamma_1^2 + 4\gamma_2\mu} > 0 \quad \text{if} \quad \mu < \frac{\gamma_1^2}{4\gamma_2}$$

The solutions of (C.7) are

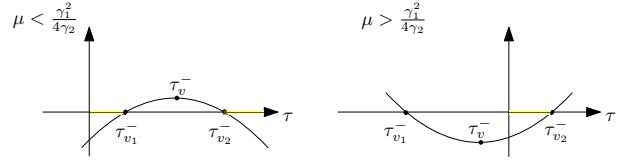


Fig. C.7. Representation of $p_v^-(\tau)$.

$$\begin{aligned} \tau_{v1}^- &= \frac{-(\gamma_1 + \alpha\mu) - \sqrt{(\gamma_1 + \alpha\mu)^2 + (-\gamma_1^2 + 4\gamma_2\mu)}}{-\gamma_1^2 + 4\gamma_2\mu} \\ \tau_{v2}^- &= \frac{-(\gamma_1 + \alpha\mu) + \sqrt{(\gamma_1 + \alpha\mu)^2 + (-\gamma_1^2 + 4\gamma_2\mu)}}{-\gamma_1^2 + 4\gamma_2\mu} \end{aligned}$$

Notice that

$$\begin{aligned} \sum \text{sol} &= \frac{\gamma_1 + \alpha\mu}{\gamma_1^2 - 4\gamma_2\mu} > 0 \quad \text{if} \quad \mu < \frac{\gamma_1^2}{4\gamma_2} \\ \prod \text{sol} &= \frac{1}{\gamma_1^2 - 4\gamma_2\mu} > 0 \quad \text{if} \quad \mu < \frac{\gamma_1^2}{4\gamma_2} \end{aligned}$$

Moreover the argument of the square root is always positive and $\tau_{v1}^- < \tau_{v2}^-$ if $\mu > \frac{\gamma_1^2}{4\gamma_2}$.

Finally, the concavity of $p_v^-(\tau)$ is upward if $\mu > \frac{\gamma_1^2}{4\gamma_2}$, otherwise it is downward. You can see these results in Fig. C.7.

In conclusion, $z^-(k_v^-, \tau)$:

$$\begin{cases} < 1 \text{ for } 0 < \tau < \tau_{v2}^- \quad \vee \quad \tau > \tau_{v1}^- & \text{if } \mu < \frac{\gamma_1^2}{4\gamma_2} \\ < 1 \text{ for } 0 < \tau < \tau_{v2}^- & \text{if } \mu > \frac{\gamma_1^2}{4\gamma_2} \end{cases}$$

- (2) $k\tau = 1$

Even if the stability analysis has been performed in the scenario where k was fixed, we will analyze the stability on the curve $k = \frac{1}{\tau}$ because the result will be useful when we will compute the convergence

rate.

$$z\left(\frac{1}{\tau}, \tau\right) = \gamma_2 \tau^2 + (\alpha + \gamma_1) \tau + \mu$$

Let us check when $z\left(\frac{1}{\tau}, \tau\right) < 1$:

$$\begin{aligned} \gamma_2 \tau^2 + (\alpha + \gamma_1) \tau + \mu &< 1 \\ \Leftrightarrow p^-(\tau) &:= \gamma_2 \tau^2 + (\alpha + \gamma_1) \tau + \mu - 1 < 0 \end{aligned}$$

$p^-(\tau)$ is an upward parabola with vertex

$$\tau_v^- = \frac{-(\alpha + \gamma_1)}{2\gamma_2} < 0$$

and solutions

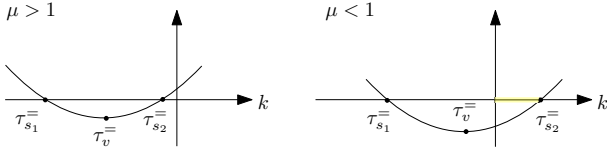


Fig. C.8. Representation of $p_s^-(k, \tau)$.

$$\tau_{s1,2}^- = \frac{-(\alpha + \gamma_1) \pm \sqrt{(\alpha + \gamma_1)^2 - 4\gamma_2(\mu - 1)}}{2\gamma_2}$$

s.t.

$$\begin{aligned} \sum \text{sol} &= -\frac{\alpha + \gamma_1}{\gamma_2} < 0 \\ \prod \text{sol} &= \frac{\mu - 1}{\gamma_2} > 0 \quad \text{if } \mu > 1 \end{aligned}$$

In conclusion:

$$z\left(\frac{1}{\tau}, \tau\right) < 1 \text{ for } \begin{cases} \nexists \tau > 0 & \text{if } \mu > 1 \\ 0 < \tau < \tau_{s2}^- & \text{if } \mu < 1 \end{cases}$$

(3) $k\tau > 1$:

Let us rewrite the function $z^+(k, \tau)$ s.t. it depends on k , since τ is assumed to be fixed now.

$$z^+(k, \tau) = \tau^2 \mu k^2 + \tau(\tau\gamma_1 + 1)k + \tau^2 \gamma_2 k + \tau\alpha - 1 \quad (\text{C.8})$$

The function represents an upward parabola with vertex

$$k_v^+ = -\frac{1 + \tau\gamma_1}{2\tau\mu} < 0 \text{ for } \tau > 0$$

Hence k_v^+ never belongs to the region $k\tau > 1$.

In conclusion $k_o(\tau) = k_v^-$ for $0 < \tau < \frac{1}{\gamma_1}$ if $\mu > \frac{1}{2}$ and for $\frac{1-2\mu}{\gamma_1} < \tau < \frac{1}{\gamma_1}$ if $\mu < \frac{1}{2}$; instead, $k_o(\tau) = \frac{1}{\tau}$ for $0 < \tau < \frac{1-2\mu}{\gamma_1}$ if $\mu < \frac{1}{2}$, that is

$$\begin{aligned} k_o(\tau; \mu, \gamma_1, \gamma_2) &= \frac{1 - \tau\gamma_1}{2\tau\mu} \quad \text{for } \tau < \frac{1}{\gamma_1} \quad \text{if } \mu > \frac{1}{2} \\ k_o(\tau; \mu, \gamma_1, \gamma_2) &= \begin{cases} \frac{1 - \tau\gamma_1}{2\tau\mu} & \text{for } \frac{1-2\mu}{\gamma_1} < \tau < \frac{1}{\gamma_1} \\ \frac{1}{\tau} & \text{for } 0 < \tau < \frac{1-2\mu}{\gamma_1} \end{cases} \quad \text{if } \mu < \frac{1}{2} \end{aligned}$$

Computation of the convergence rate

The convergence rate, defined in (29), corresponds to the function $z(k, \tau)$ evaluated in $\tau = \tau_o(k)$:

$$\rho(\tau) = z(k_o, \tau)$$

We have already seen that, depending on the value of the parameter μ , then $k_o(\tau)$ has different values and $z(k_o(\tau), \tau)$ too:

- $0 < \mu < \frac{1}{2}$:

$$k_o = \begin{cases} k_v^- & \text{for } \frac{1-2\mu}{\gamma_1} < \tau < \frac{1}{\gamma_1} \\ \frac{1}{\tau} & \text{for } 0 < \tau < \frac{1-2\mu}{\gamma_1} \end{cases}$$

and

$$\begin{aligned} \rho(\tau) &= z^-(k_o, \tau) = \\ &= \begin{cases} z^-(k_v^-, \tau) & \text{for } \frac{1-2\mu}{\gamma_1} < \tau < \frac{1}{\gamma_1} \\ z\left(\frac{1}{\tau}, \tau\right) & \text{for } 0 < \tau < \frac{1-2\mu}{\gamma_1} \end{cases} \\ &= \begin{cases} \frac{(-\gamma_1^2 + 4\gamma_2\mu)\tau^2 + 2(\gamma_1 + 2\alpha\mu)\tau + 4\mu - 1}{4\mu} & \text{for } \frac{1-2\mu}{\gamma_1} < \tau < \frac{1}{\gamma_1} \\ \gamma_2 \tau^2 + (\alpha + \gamma_1) \tau + \mu & \text{for } 0 < \tau < \frac{1-2\mu}{\gamma_1} \end{cases} \end{aligned}$$

- $\mu > \frac{1}{2}$: in this case

$$\begin{aligned} \rho(\tau) &= z^-(k_v^-, \tau) = \\ &= \frac{(-\gamma_1^2 + 4\gamma_2\mu)\tau^2 + 2(\gamma_1 + 2\alpha\mu)\tau + 4\mu - 1}{4\mu} \\ &\text{for } 0 < \tau < \frac{1}{\gamma_1} \end{aligned}$$

D Online Gain Design Proposed in [21]

Let us introduce the following auxiliary system,

$$\begin{aligned} \dot{\mathbf{q}}'(\tau; \mathbf{q}_h) &= -\mathbf{A}_{\mathbf{q}'(\tau; \mathbf{q}_h)}^{-1} \mathbf{A}_{\mathbf{q}_h} \mathbf{q}_h =: \mathbf{f}(\mathbf{q}'(\tau); \mathbf{q}_h) \quad (\text{D.1}) \\ \mathbf{q}'(0; \mathbf{q}_h) &= \mathbf{q}_h; \quad \mathbf{q}_h \in \mathcal{B}_d(\mathbf{q}^r), \end{aligned}$$

with $\mathbf{q}_h \stackrel{\text{def}}{=} \mathbf{q}(hT)$. Being $\mathbf{f}(\mathbf{q}; \mathbf{q}) = -\mathbf{q}$, it holds $\|\mathbf{q}'(0^+; \mathbf{q}_h) - \mathbf{q}^r\| < \|\mathbf{q}_h - \mathbf{q}^r\|$. Also, we define

$$\tau_s(\mathbf{q}_h) \stackrel{\text{def}}{=} \min_{\tau} \{\tau < 0 \mid \|\mathbf{q}'(\tau; \mathbf{q}_h)\| = \|\mathbf{q}_h\|\}, \quad (\text{D.2})$$

$$\tau_o(\mathbf{q}_h) \stackrel{\text{def}}{=} \operatorname{arginf}_{0 \leq \tau \leq \tau_s(\mathbf{q}_h)} \|\mathbf{q}'(\tau; \mathbf{q}_h)\|, \quad (\text{D.3})$$

where $\tau_s(\mathbf{q}_h) = \infty$ if $\|\mathbf{q}'(\tau; \mathbf{q}_h) - \mathbf{q}^r\| < \|\mathbf{q}_h - \mathbf{q}^r\|, \forall \tau$. Then, k_h is designed as (see [21, Proposition 7])

$$k_h = \frac{\tau_o(\mathbf{q}_h)}{T}. \quad (\text{D.4})$$

E Additional Simulations

In Fig. E.1, we show the behavior of the system state when increasing the noise variance of the sensor that collects data from the MoCap system. $\sigma_2 = 0.003$ is the variance used for the previous simulations, while $\sigma_1 = 0.01$ is the one used for this simulation. You can notice that, as expected, the performance become worse when increasing the noise variance and the oscillations around the reference trajectory become bigger. This result shows that our strategy can handle uncertain measurements of the state \mathbf{q} while guaranteeing stability of the system.

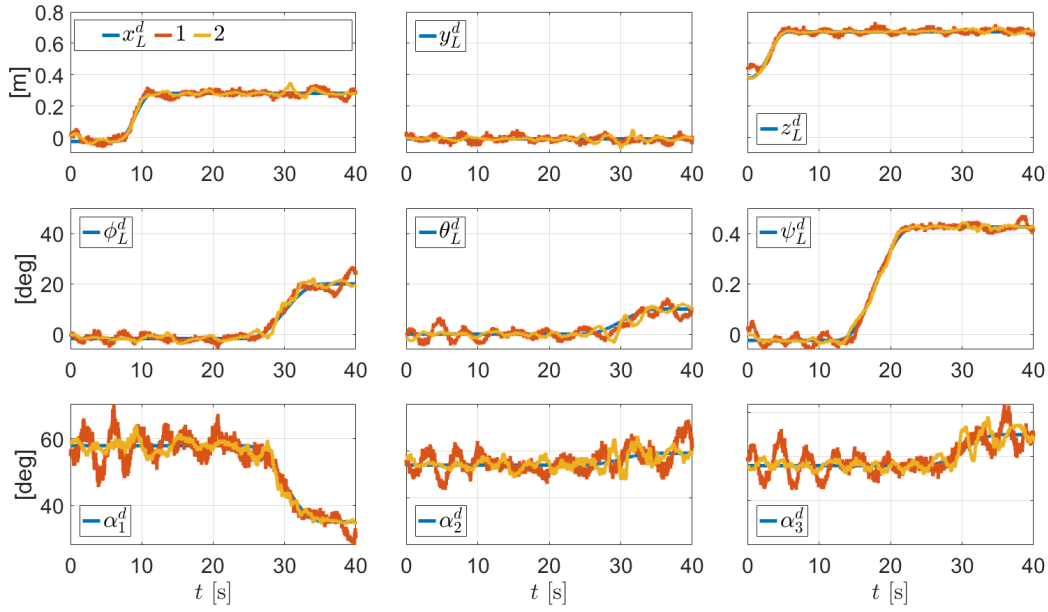


Fig. E.1. Comparison of the variables $\mathbf{q}(t)$ for two different values $\sigma_1 = 0.01$ and $\sigma_2 = 0.003$ of noise variance of the sensor vision (the values 1 and 2 in the legend refer to $\sigma_{1,2}$): the tracking strategy SIKM-D is implemented with sampling time $T = 0.75$ [s] and feedback gain $k_{\text{off}} = 1.28$. The first two rows represent respectively the position x_L, y_L, z_L and orientation ϕ_L, θ_L, ψ_L (roll, pitch and yaw) of the load. On the last row the angles $\alpha_i \stackrel{\text{def}}{=} q_i, i = 1, 2, 3$ between the cables and the load are depicted. Notice that the oscillations around the reference trajectory become bigger as the noise variance increases.